The Canadian Mineralogist
Vol. 50, pp. 219-233 (2012)
DOI: 10.3749/canmin.50.2.219

CRYSTAL CHEMISTRY AND ELECTRICAL CONDUCTIVITY OF BOULANGERITE, DADSONITE AND IODINE-SUBSTITUTED PILLAITE GROWN BY CHEMICAL VAPOR TRANSPORT

RONNY KADEN[§], GERALD WAGNER AND KLAUS BENTE

Institute of Mineralogy, Crystallography and Materials Science, Scharnhorststr. 20, D–04275 Leipzig, Germany

ABSTRACT

Experimental results are presented concerning the synthesis, crystal chemistry and electrical characterization of Pb–Sb–S sulfosalts, especially boulangerite, $Pb_5Sb_4S_{11}$. The crystals were grown by sublimation or chemical vapor transport using NH_4Cl or iodine as transporting agents. Owing to its rod-like structure, boulangerite typically appears as thin needles as well as fibers with diameters down to a few nanometers. Both ordered as well as disordered structures can be produced depending on growth temperature. In addition, depending on the temperature of deposition, $Pb_2Sb_2S_5$ or halogen-bearing sulfosalts such as dadsonite or iodine-substituted pillaite can be prepared as well. By means of thermodynamic modeling, the chemical vapor-transport reaction of boulangerite is described, and an explanation for the formation of the halogen-containing compounds at lower temperatures of deposition is given. Within the homogeneity range of boulangerite $Pb_{5-x}Sb_{4+x}S_{11+x/2}$ with $0.35 \geq x \geq -0.09$, the electrical conductivity σ reaches values between 10^{-8} and 10^{-3} $\Omega^{-1}m^{-1}$. For $Pb_2Sb_2S_5$, iodine-substituted pillaite and dadsonite, σ was determined to be $2.0(8) \times 10^{-4}$, $5(2) \times 10^{-4}$ and $7(3) \times 10^{-4}$ $\Omega^{-1}m^{-1}$, respectively.

Keywords: sulfosalts, boulangerite, dadsonite, pillaite, synthesis, chemical vapor transport, OD structure, nonstoichiometry, electrical conductivity.

INTRODUCTION

In recent years, complex sulfosalts have become objects of interest as alternative semiconducting materials for thermoelectric or phase-change-based memory applications. Moreover, owing to their electronic attributes such as E_g in the range of 1.1–2 eV and an optical absorption α of $10^4 - 10^5$ cm^{-1} (Dittrich & Herz 1998, Dittrich *et al.* 2007, 2009), they should be particularly suitable as absorbers in solar cells (photovoltaics, PV). On the other hand, self-assembled arrangements of wires or rods for sensor devices and nanotechnology are required (Cui *et al.* 2001, Yi *et al.* 2002, Duan *et al.* 2003, Leontidis *et al.* 2003). Therefore, we selected boulangerite, ideally $Pb_5Sb_4S_{11}$, a phase in the system $PbS–Sb_2S_3$, because its E_g of 1.34 eV (Boldish & White 1998) or 1.47 eV (Lomelino & Mozurkewich 1989) lies near the optimum for conversion of solar energy (Dittrich *et al.* 2007). Telkes (1950) reported negative Seebeck coefficients of –135 up to –900 μV/K, *i.e.*, n-type conductivity, which indicates a probable potential in thermoelectrics (TE) also. Owing to its chain-like crystal structure (Born & Hellner 1960), boulangerite commonly appears in nature as thin needles or wires up to several centimeters in length, or in some cases as coils of wires. This propensity to one-dimensional crystal growth favors boulangerite for self-assembled arrangements of micro- or nanowires. However, the serious drawback for applications in PV or TE is the rather poor electrical conductivity of boulangerite, about 10^{-6} $\Omega^{-1}m^{-1}$ (Lomelino & Mozurkewich 1989). As reported by Dittrich *et al.* (2007), amorphous or polycrystalline thin films of $PbS–Sb_2S_3$ sulfosalts show values between 10^{-4} and 10^4 $\Omega^{-1}m^{-1}$. As boulangerite can be Sb-rich, *i.e.,* in the homogeneity range $Pb_{5-x}Sb_{4+x}S_{11+x/2}$ (Salanci 1979, Moh *et al.* 1991), a composition-dependent variation of the electrical conductivity, σ, is expected.

Studies on phase relations in the system $PbS–Sb_2S_3$ have been already made by numerous authors, as summarized by Kitakaze *et al.* (1995), whereas the most comprehensive findings can be attributed to Salanci (1979) and Wang (1973, 1976). The crystal chemistry and structures of individual sulfosalt phases, as well as a systematic review of the structural aspects, were published by Skowron & Brown (1994). Structural principles in homologous sulfosalt systems were discussed

§ *Current address*: Martin-Luther-University Halle/Wittenberg, Institute of Geosciences and Geography, Departement of Mineralogy–Geochemistry, Von Seckendorff Platz 3, D–06120 Halle (Saale), Germany. *E-mail address*: ronny.kaden@geo.uni-halle.de

by Andersson & Hyde (1974), Hyde *et al.* (1974), Makovicky & Karup-Møller (1977a, 1977b), Makovicky (1977, 1985, 1989, 1993) and Makovicky & Topa (2009). Single needle-shaped crystals of boulangerite have successfully been grown by vapor transport with iodine (Skowron & Brown 1990a, Moh *et al.* 1991) or without a transporting agent (Lomelino & Mozurkewich 1989). Nevertheless, there are no reports of the growth of boulangerite *via* chemical vapor transport (CVT) using NH_4Cl, and about the degree of metal order in such synthetic boulangerite, as is found for natural specimens. An exception was the TEM examination of melt-grown boulangerite (Heuer *et al.* 2004), which revealed a statistical distribution of metals probably due to the high temperature of the process. Transport experiments with iodine at lower temperatures, 380°C, did not lead to boulangerite (Kryukova *et al.* 2005). Chemical vapor-transport experiments *via* NH_4Cl were described in the system $PbS–Bi_2S_3$ by Carlson (1972) and for troilite (FeS) by Krabbes *et al.* (1976). So far, systematic details on the CVT synthesis of single crystals of boulangerite of different nonstoichiometries are missing. Thus, in this paper, we report on the CVT synthesis, structural characterization of boulangerite and the effect of variable Pb:Sb ratio on its electrical conductivity, together with the examination of associated halogeno-sulfosalts like dadsonite and the iodine derivative of pillaite.

Experimental

The samples of boulangerite come from the mines of Trepça, in the Republic of Kosovo, and Příbram, in the Czech Republic. The crystals of synthetic boulangerite were prepared by CVT in evacuated and fused silica tubes. For CVT, the ampoules were placed in a tube furnace with a parabolically decreasing temperature profile from T_{source} to (T_{source} – 37 K). The transport distance and the inner tube diameter were kept constant at 100 mm and 12 mm, respectively. We added NH_4Cl to create the transporting agent HCl. The source material for CVT experiments was synthesized by solid-state reaction in fused silica tubes starting with pure elements Pb, Sb, and S (purity better than 99.995%). At first, the mixtures were treated for five days at T = 250°C, followed by a slow heating up to 850°C (50 degrees per day), to obtain a homogeneous melt. This melt was quenched to room temperature by switching off the furnace. After grinding, the powder was pressed to pellets, which were treated again in fused silica tubes at 570°C for seven days, followed by rapid quenching in air. This as-grown material served as a source for CVT. The chemical vapor-transport process was thermodynamically modeled by the CVTrans software (Glaum *et al.* 1997).

The X-ray-diffraction data were collected from powder samples with Cu*K*α radiation (λ = 0.1541874 nm) in an X'Pert Pro Diffraktometer system (PANalytical) in a range of $5° \le 2\theta \le 90°$ (step size 0.016°, t = 20 s) operating in Bragg–Brentano geometry with an X'Celerator RTMS detector. For phase analysis and Rietveld refinement, the software X'Pert HighScore Plus (PANalytical 2009) was used, and silicon served as an internal standard.

The morphology and dimensions of the samples were studied using a Zeiss DSM 640 scanning electron microscope (SEM) operating at 15 kV, 20 μA. For HRTEM analysis, the crystals were stuck between GaAs wafers used as a dummy material. In this way, sections were prepared with the boulangerite crystal fibers cut along and across their elongation. After mechanical grinding and polishing, the specimens were thinned by Ar^+ ion milling in a GATAN Duo-Mill. Typical operating conditions were 4 kV, 0.5 mA and an incident angle of the beam of about 11°–13°. Selected-area electron-diffraction patterns (SAED) and HRTEM images were obtained using a Philips CM–200 STEM equipped with a super twin objective lens (point resolution 2.3 nm). The HRTEM image simulations and the calculation of the SAED pattern were made by means of the JEMS software (Stadelmann 1987, 2008). The composition of the crystals was determined by a calibrated EDX system (EDAX) adapted to the CM200 STEM used.

To measure the electrical conductivity, single crystals of boulangerite were fixed on an isolating substrate using Ga–In alloy to ensure ohmic point-contacts at each end of one individual needle. The measurements of the current–voltage characteristics were carried out with an Agilent 4156C Precision Semiconductor Parameter Analyser using a SÜSS MicroTec Waferprober for the contacts.

The Crystal Structure of Boulangerite and Degree of Metal Order

As is typical for sulfosalts, the crystal structure of boulangerite consists of structural fragments derived from the herzenbergite (SnS) archetype (Makovicky 1993). In case of boulangerite, three parallel Me_6S_8 ribbons form rhombic building blocks with chain-like extension along the needle axis, *i.e.*, the crystallographic **c** axis (Fig. 1). Although there are different unit-cell settings in literature, we assign our data to the orthorhombic basic cell after Moh *et al.* (1991) or Petrova *et al.* (1978), with *a* 21.240, *b* 23.510, *c* 4.036 Å, as a convention for comparison. The three marginal metal sites of each of the two external ribbons are occupied by Pb only. Two of the inner metal sites are completely occupied by Sb, whereas the third one is partially replaced by Pb. The metal sites of the central ribbon are mixed (Pb,Sb) sites. Two types of OD structures result. The first type has a statistical metal distribution with site-occupancy factors (Pb) of 0.45–0.60 on the mixed sites (Petrova *et al.* 1978). In the other type, these mixed sites can be ordered, with ideally a complete

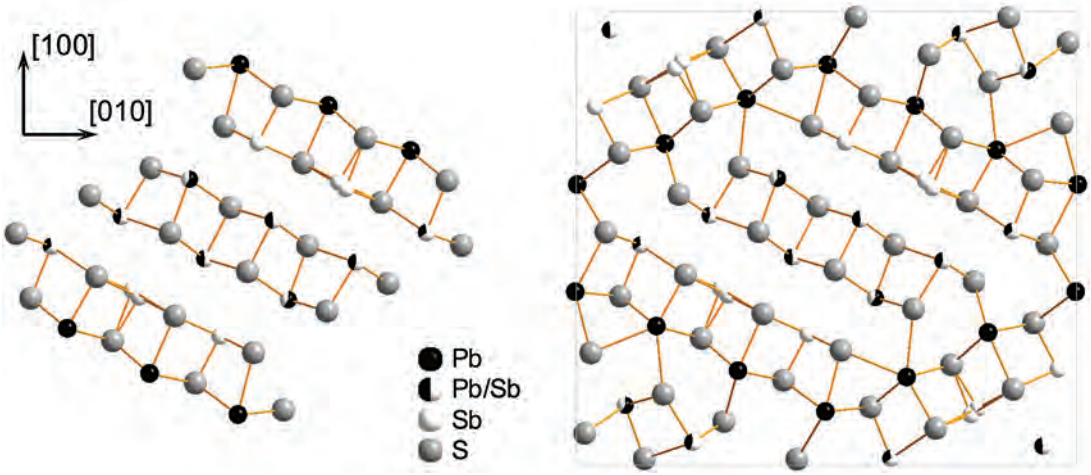

FIG. 1. The orthorhombic structure of boulangerite, with a statistical distribution of metals (Moh *et al.* 1991) projected along [001], *i.e.*, a cross-section of a needle. Left: the fundamental building-block unit composed of three Me_6S_8 ribbons with infinite extension along the viewing direction [001]. Right: the unit cell.

occupancy of Pb or Sb alternating in the **c** direction, leading to the doubling of the *c* parameter. In addition, the occupancy of these metal sites alternates in the **a** direction as well. Therefore, the whole ordered structure leads to a supercell of $2a \times b \times 2c$ with a basal face-centering of (010), first reported by Born & Hellner (1960). This coupled alternation can also be described with a monoclinic unit-cell with *a* 21.612, *b* 23.543, *c* 8.084 Å, and β 100.70°, as reported by Mumme (1989). As the *c* parameter is doubled, $\vec{c}^{\ \mathrm{mon}} = 2\,\vec{c}^{\ \mathrm{ortho}}$, and as the monoclinic **a** axis is directed to the face centering of the supercell $\vec{a}^{\ \mathrm{mon}} = \vec{a}^{\ \mathrm{ortho}} + \vec{c}^{\ \mathrm{ortho}}$, the monoclinic inclination β results.

THE SYNTHESIS OF BOULANGERITE BY CHEMICAL VAPOR TRANSPORT

For the synthesis of boulangerite, the general formula of the reactant was taken as $Pb_{5-x}Sb_{4+x}S_{11+x/2}$, in agreement with the composition range due to Sb excess as reported by Salanci (1979). To check for a possible extension of this solid solution toward Pb-rich compositions, negative steps of $(-x) = 0, 0.1, 0.2, 0.3, 0.4, 0.5$ were also prepared. Of special interest was a test to see if the mineral "falkmanite", described by Hiller (1939) and Ramdohr & Ödman (1940), does exist. Robinson (1948) and Hiller himself (*cf.* Fleischer 1955) doubted its existence and concluded that it is boulangerite. Later Mozgova *et al.* (1983), McQueen (1987) and Pruseth *et al.* (2001) reported again on the existence of "falkmanite", but convincing evidence by crystal-structure data is still missing (Moëlo *et al.* 2008).

Thus, after the synthesis of the above-mentioned compositions by solid-state reaction and a final annealing at T = 570°C (ten days), the material was quenched to room temperature to freeze in the thermodynamic equilibrium at these conditions. Our XRD analyses of this material revealed that all samples are boulangerite in association with some additional galena, the proportion of which increases with increasing $(-x)$. Other phases, like Cu-free meneghenite or "falkmanite", were not detected.

The chemical vapor transport (CVT) was carried out as described in the experimental section. The duration of transport was kept at seven days. The maximum temperatures, 637°C in the source area and 600°C in deposition zone, are near the melting point of boulangerite (631°C: Salanci & Moh 1970). Owing to the decomposition of NH_4Cl, releasing the transporting agent HCl, additional N_2, H_2 and minor amounts of NH_3 are formed under thermodynamic equilibrium conditions assumed at the given temperatures (Krabbes *et al.* 1976, Dirtu *et al.* 2006).

To understand how the CVT process of boulangerite works near the conditions of thermodynamic equilibrium, the mass transfer was modeled using the program CVTRANS (Glaum *et al.* 1997). It combines the G_{min} method (Eriksson 1971) with the cooperative transport model (Gruehn & Schweizer 1983). Therefore, the thermochemical data for the condensed phases PbS, Pb, $PbCl_2$, Sb_2S_3, Sb, $SbCl_3$ and about 50 gaseous species (Binnewies & Milke 1999, Knacke *et al.* 1991, JANAF 1986, Barin 1992, Kubaschewski & Alcock 1983) have been considered.

Because the thermochemical data for different compositions of boulangerite are not available, they were calculated as those of a true mixture according to Craig & Lees (1972) and Craig & Barton (1973). The latter item gives the standard-state enthalpy and entropy of $Pb_5Sb_4S_{11}$ as a mixture of PbS, Sb and sulfur, but values of the heat capacity for temperature-dependent calculations are missing. However, considering the structural building principles of sulfosalts derived from the archetype herzenbergite, boulangerite, ideally $Pb_5Sb_4S_{11}$, was approximated to the formula $Pb_{5-x}Sb_{4+x}S_{11+x/2}$ which is a mixture of $(5-x)$PbS + $(4+x)$ $SbS_{1.5}$, *i.e.*, $(5-x)$PbS + $(2+½x)Sb_2S_3$, where Pb and Sb are in a coordination and chemical bonding environment as in PbS and Sb_2S_3, respectively. Therefore, the heat capacity of the compound boulangerite $C_p(B) = \sum_i C_p(i) \bullet x_i$ can be assumed to be the sum of the fractional $C_p(i)$ of the components i (PbS and $SbS_{1.5}$) in their molar fractions x_i with:

$$C_p(i, T) \bullet x_i = A \bullet x_i + B \bullet T \bullet x_i + C \bullet 1/T^2 \bullet x_i + D \bullet T^2 \bullet x_i. \quad (1)$$

Using the common relations, the standard enthalpy of formation $\Delta_f H^0_T$ and entropy $\Delta_f S^0_T$ of the compound boulangerite can be calculated. Deviating from the model of Craig & Barton (1973), which applies a factor of 1.2 ± 0.8 in the entropy term of the free mixing enthalpy ΔG_m, the non-ideal mixing in this approach is expressed by W for the enthalpy of mixing $\Delta_{mix} H^0_T(i)$:

$$\Delta_{mix} H^0(i) = W \bullet x_{PbS} \bullet x_{SbS1.5} \quad (2)$$

Thus, the standard Gibbs energy of the real mixture can be derived from the standard state Gibbs energy of an ideal mixture $\Delta G_f(B)^{real} = \Delta G_f(B)^{ideal} + \Delta_{mix} H^0_T(I)$:

$$\Delta G_f(B)^{real} = \sum_i \Delta_f H^0_T(i) \bullet x_i - T \bullet \left[\sum_i S^0_T(i) \bullet x_i \; R \bullet \sum_i \left(x_i \bullet \ln x_i\right)\right] + \Delta_{mix} H^0_T(i) \quad (3)$$

In this way, the thermochemical data for boulangerite $Pb_{5-x}Sb_{4+x}S_{11+x/2}$ with reasonable values of x were estimated. The first successful calculations with CVTRANS could be performed with a lowest absolute W value of –123 kJ/mol, which results in a mixing enthalpy of about –25 kJ/mol. These values fit well the range of energies reported by Ghosal & Sack (1999) for non-ideal mixing in Ag–Sb–Bi sulfosalts. The initial values of enthalpy, entropy and heat capacity increments for PbS and Sb_2S_3 were taken from Binnewies & Milke (1999). The calculated standard enthalpies, entropies and Gibbs free energies for different compositions of boulangerite are listed in Table 1. They seem to be reasonable compared to the values for sulfosalt ore minerals given by Craig & Lees (1972) and Craig & Barton (1973).

The composition range $-0.5 \le x \le 0.5$ considers the suggested boulangerite homologue series with the end members "falkmanite" $Pb_{5.5}Sb_{3.5}S_{10.75}$ and "plumosite" $Pb_2Sb_2S_5$ (Mozgova & Bortnikov 1980, Mozgova *et al.* 1984, Vrublevskaja *et al.* 1985, McQueen 1987, Mumme 1989). However, according to Moëlo *et al.* (2008), both end members are not established mineral species. Nevertheless, our calculated data attest that all compounds of this homologous series have roughly the same thermodynamic stability, owing to nearly equal values of the negative Gibbs energy. However, the values of the negative Gibbs energy increase slightly for boulangerite with a deficiency in Pb. Therefore, Pb-poor compositions should be thermodynamically favored with respect to Pb-rich ones. This is in good agreement with the homogeneity range of boulangerite $Pb_{5-x}Sb_{4+x}S_{11+x/2}$ found by Salanci (1979), which allows a Pb deficiency up to $x \approx 0.3$.

The gaseous species could be reduced to about 32 probable ones (see Fig. 2a) with different thermochemical data in some cases. If the data given by Binnewies & Milke (1999) and Knacke *et al.* (1991) are used, then the calculated results match well the experimental ones. It follows that HCl, H_2S, SbCl, $PbCl_2$ and $SbCl_3$ are dominantly responsible for the mass transfer j, as demonstrated in Figure 2a. Sublimated sulfides, such as PbS, Pb_2S_2, SbS, Sb_2S_3 play a subordinate role. Confirming the experimental results, the decrease of $SbCl^{gas}$ and $PbCl_2{}^{gas}$ with lowering temperature suggests that the transporting reaction must be endothermic. Moreover, the partial pressure of $SbCl^{gas}$ is larger than for $PbCl_2{}^{gas}$. This favors the mass transfer of Sb over Pb and, therefore, the crystallized boulangerite has a lower content of Pb than the starting material. This is actually observed in all experiments (Table 2) and is in agreement with the calculated thermochemical data mentioned above. In addition, the calculated composition of the source (Fig. 2b) predicts the coexistence of a rather Pb-poor boulangerite in addition to galena

TABLE 1. CALCULATED THERMOCHEMICAL DATA FOR VARIOUS COMPOSITIONS OF BOULANGERITE AT T = 25°C

Pb	Sb	S	$\Delta_f H^o_T$	$\Delta_f H^o_T + \Delta_{mix} H^o_T$	$\Delta_f S^o_T$	$\Delta_f G^{real}$	C_p factors	
apfu			kJ/mol	kJ/mol	J/mol	kJ/mol	A	B•10^{-3}
5.5	4.5	10.75	-899.4	-928.6	826.2	-1174.8	435.3	157.7
5.4	3.6	10.8	-899.8	-929.3	826.2	-1175.6	435.7	159.8
5.2	3.8	10.9	-900.7	-930.7	826.2	-1176.9	436.5	164.0
5	**4**	**11**	**-901.5**	**-931.9**	**826.2**	**-1178.1**	**437.4**	**168.1**
4.8	4.2	11.1	-902.3	-933.0	826.2	-1179.2	438.2	172.3
4.6	4.4	11.2	-903.2	-933.9	826.1	-1180.1	439.1	176.5
4.5	4.5	11.25	-903.6	-934.4	826.1	-1180.5	439.5	178.6

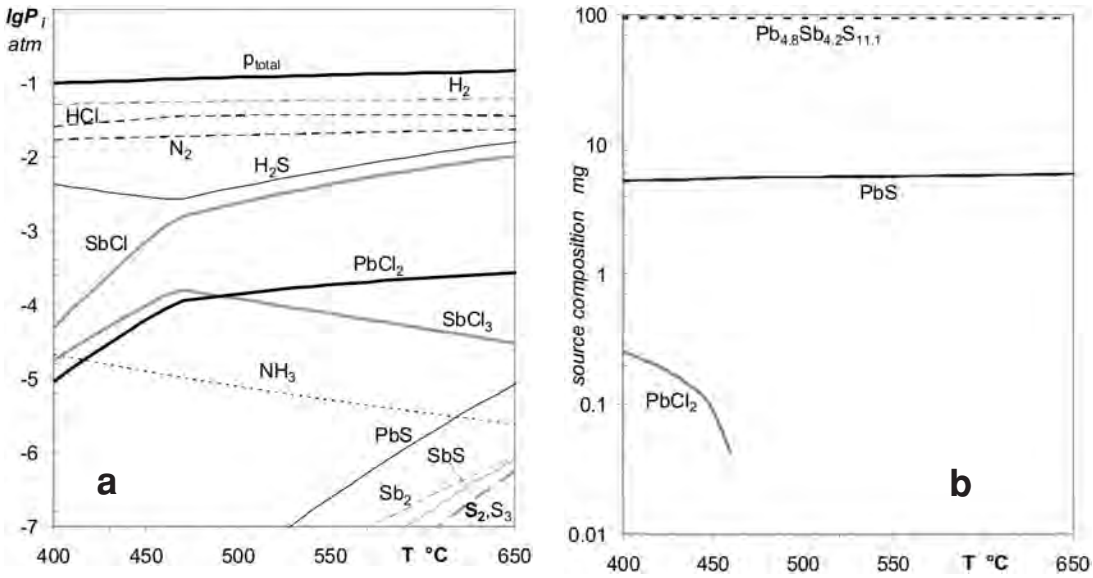

FIG. 2. a) Vapor phases in equilibrium with 100 mg boulangerite $Pb_5Sb_4S_{11}$ and 0.4 mg NH_4Cl per 12 mL volume at an initial pressure $P_0^{25°C}$ of 0.001 atm, calculated by the CVTRANS software (Glaum *et al*. 1997), by application of thermochemical data for condensed phases (PbS, Pb, $PbCl_2$, *Sb_2S_3, Sb and #$Pb_5Sb_4S_{11}$) and gaseous species (N_2, N, H_2, H, NH_3, N_2H_2, HCl, Cl_2, Cl, H_2S, HS, H_2S_2, Pb, PbS, Pb_2S_2, *$PbCl_2$, *$PbCl_4$, Sb, Sb_2, SbS, Sb_2S_3, SbCl, *$SbCl_3$, *$SbCl_5$, S_1,…,S_8) after Binnewies & Milke (1999) or *Knacke *et al*. (1991). #The thermochemical data for boulangerite were calculated. b) Corresponding source-masses calculated for equilibrium conditions.

TABLE 2. TEM–EDX ANALYSIS OF *NATURAL AND SYNTHETIC CRYSTALS OF BOULANGERITE

sample	reactant $Pb_xSb_yS_{x+1.5y}$			NH_4Cl	T_{growth}	mass transfer *j*	phase deposited	Pb	Sb	S_{EDX} / S_{ideal}	Pb:Sb
	Pb	Sb	S	mg/mL	°C	mg/h	(XRD)	formula units per 9 metal atoms			at. ratio
* Trepça	---	---	---	---	---	---	---	5.03(8)	3.97(8)	11.11(26) / 10.98	1.26(4)
* Příbram	---	---	---	---	---	---	---	4.88(7)	4.12(7)	11.05(54) / 11.07	1.18(4)
B8-F	5.2	3.8	10.9	0.033	600°	0.34(1)	boulangerite	4.89(7)	4.11(7)	11.71(32) / 11.06	1.19(4)
B8-C	5	4	11	0.033	600°	0.32(1)	boulangerite	4.77(7)	4.23(7)	11.49(26) / 11.12	1.13(4)
° XE8D	5	4	11	---	570°	*resubl.*	boulangerite	5.00(9)	4.00(9)	11.88(34) / 11.00	1.26(4)
B8-G	5.5	3.5	10.75	0.033	570°	0.22(2)	boulangerite	5.09(9)	3.91(9)	11.30(47) / 10.94	1.30(4)
B8-D	5.2	3.8	10.9	0.033	570°	0.22(2)	boulangerite	5.04(8)	3.96(8)	10.87(17) / 10.98	1.27(4)
B8-A	5	4	11	0.033	570°	0.18(2)	boulangerite, ^{v} $Pb_2Sb_2S_5$	4.82(9)	4.18(9)	12.53(40) / 11.09	1.16(4)
EL81	5.3	3.7	10.85	<0.02	570°	0.10(1)	boulangerite	4.65(6)	4.35(6)	10.79(24) / 11.18	1.07(4)
EL82	5.3	3.7	10.85	<0.02	570°	0.11(1)	boulangerite	4.67(6)	4.33(7)	11.10(25) / 11.17	1.08(4)
EL83	5.3	3.7	10.85	<0.02	570°	0.12(1)	boulangerite	4.69(8)	4.31(8)	11.41(27) / 11.16	1.09(4)
B8-B	5	4	11	0.033	470°	0.02(1)	^{v} $Pb_2Sb_2S_5$	2.03(2)	1.97(2)	5.13(18) / 5	1.03(4)
XE8A	5	4	11	0.033	450°	0.03(1)	dadsonite	$Pb_{24}Sb_{20.5}S_{54}Cl_{1.5}$			1.17(4)
XE8C	5	4	11	iodine	450°	0.13(1)	I-doped pillaite, PbS	$Pb_{9.6}Sb_{7.9}S_{23}I_{1.55}$			1.22(4)

Synthetic boulangerite grown by CVT for a temperature gradient of about 37 K and growth time of 7 days. ° XE8D: crystallization on educt at 570°C, 7d; ^{v} $Pb_2Sb_2S_5$: phase V (Salanci 1979); *resubl.*: resublimation. For each sample, about 12 spectra of different needles were collected. The standard deviations are given in brackets. The determination of specimen composition was done using calibrated TEM–EDX considering the S*K*α, Pb*L*α, Pb*M*α, and Sb*K*α lines. The ratio Pb:Sb was accurately determined from Pb*L*α and Sb*K*α lines. Note that S*K*α, as the only spectral line of sulfur, overlaps with the Pb*M*α line. This leads to slight deviations in the values of the atomic ratio Pb:S, in spite of the calibrated Cliff–Lorimer factors.

owing to the greater solubility of Sb than of Pb in the vapor phase.

For a starting composition of stoichiometric $Pb_5S_4S_{11}$, the whole mass-transfer and the transfer of lead relative to that of antimony decrease with decreasing temperature (samples B8–C, –A, –B). Only a deposition at 600°C leads to pure boulangerite, which has a lead deficiency (Table 2). For even lower temperatures of deposition (570° and 470°C), crystallization of $Pb_2Sb_2S_5$ occurred (sample B8–A and –B in Table 2). This phase can be attributed to the "phase V" described by Salanci (1979). The crystallization of this compound at 570°C lies inside the reported range of stability between 506° and 598°C (Salanci 1979), or between 490° and 584°C (Kitakaze *et al*. 1995), whereas the deposition at 470°C lies a little below. Without any transporting agent, no significant mass-transfer was observed, although needles of stoichiometric boulangerite crystallized on the stoichiometric source material $Pb_5S_4S_{11}$ (T_{growth} = 570°C) by simple resublimation (sample XE8D in Table 2).

To enable the deposition of boulangerite with a higher Pb content, the source material needs to be enriched with lead. For a constant concentration of NH_4Cl, a considerable excess of Pb in the source material is needed for the formation of Pb-rich boulangerite (*cf*. samples B8 –G and –D in Table 2).

Calculating the vapor-phase equilibrium by CVT for temperatures below T = 470°C, the concentrations of Cl-bearing gaseous species are reduced, owing to the formation of $PbCl_2$ as a liquid condensed phase. Although we did not observe any $PbCl_2$, a Cl-bearing sulfosalt like dadsonite $Pb_{24}Sb_{20.5}S_{54}Cl_{1.5}$ (T_{dep} = 450 °C) did form; it differs slightly in Pb:Sb ratio and Cl content from the structures reported by Makovicky *et al*. (2006). Moreover, in analogous CVT runs using iodine as transporting agent, iodine-substituted pillaite, $Pb_{9.6}Sb_{7.9}S_{23}I_{1.55}$ (see Kryukova *et al*. 2005) formed at $T_{dep} \leq 450$°C, indicating a similar good affinity of Pb for I.

Synthetic roughly stoichiometric boulangerite grows as needles, 1–10 mm in length and only a few 10 μm in width (Fig. 3a). Lead-poor boulangerite appears as flat lamellae, which consist of individual fibers in parallel intergrowth along the needle axis [001] (Fig. 3b). The CVT-grown dadsonite and iodine-substituted pillaite have similar morphologies as boulangerite, whereas their mosaic-like intergrowth leads to hollow needles or wires (Figs. 3c, d).

Compared to synthetic products, the atomic ratio Pb:Sb of boulangerite can also differ from that of the ideal composition $Pb_5Sb_4S_{11}$, depending on the provenance, as listed in Table 2. In particular, values less than 1.25, *i.e*., cases of Pb-poor boulangerite, are observed. Whereas slightly Pb-rich needle-shaped boulangerite (length up to a few cm) associated with PbS is characteristic for Trepça (Table 2), the boulangerite needles from Příbram are rather Pb-poor, without galena.

Transmission Electron Microscopy and Microstructure

As SEM imaging revealed, the boulangerite samples as well as the halogen-bearing sulfosalt needles consist of microfibers in strongly parallel intergrowth. Transmission electron microscopy confirmed that these fibers are differently twisted in azimuth, forming a mosaic-like texture, which causes a quasi-powder pattern in single-crystal X-ray diffraction. Therefore, the microstructure and the state of metal order of the individual fibers are the object of consideration by HRTEM and SAED.

All of the natural boulangerite samples, from Trepça and Příbram, exhibit a particularly strong degree of metal order, causing additional rows of bright spots (see arrows in Fig. 4) in SAED pattern containing the **c*** direction. These spots appear at the half-position along the **c*** direction between the reflection rows (arrow tips) of the orthorhombic basic cell with a statistical metal distribution. In addition, these spots are shifted by ½•a*, which results in the inclination β = 100(1)° of the monoclinic unit-cell with ordered metal distribution (see inset in Fig. 4b). In the HRTEM lattice image, this metal order is reflected by bright contrasts in the corresponding symmetry (Fig. 4b). The additional spots in the SAED pattern of synthetic boulangerite (Fig. 4c) are rather weak compared to those of the natural ones (Fig. 4b), which appear with nearly the same intensity as the reflections of the orthorhombic basic structure. The weaker additional spots for stoichiometric specimens (B8–D) or slightly Sb-rich ones (B8–A, –C, –F) indicate only an imperfect degree of order, as shown for example in Figure 4c.

In contrast to nonstoichiometric boulangerite, in the stoichiometric sample XE8D, which crystallized without any transporting agent, the reflections caused by metal order degenerate to diffuse streaks (Fig. 4d). The same behavior can be observed if the atomic ratio Pb:Sb is strongly decreased (samples EL81–3). Thus the degree of metal order is marginal. However, the diffraction pattern of Pb-rich boulangerite sample B8–G does not show any additional reflections, evidence of statistical occupancy of metal sites. Therefore, we conclude that an excess as well as a strong deficiency of lead makes metal ordering very difficult.

A credible explanation for the weaker degree of metal order is the short time taken for formation compared to natural boulangerite. Owing to the conditions of hydrothermal growth at elevated temperature (and pressure) over a long term, the highly ordered distribution of metals in natural boulangerite represents the thermodynamic equilibrium state. Apparently, the absolute temperature of growth seems to play a subordinate role. Ordered natural crystals that were annealed at 550°C for two weeks in evacuated silica tubes show the same degree of metal order as before. In contrast, the period of CVT synthesis is comparatively short (seven

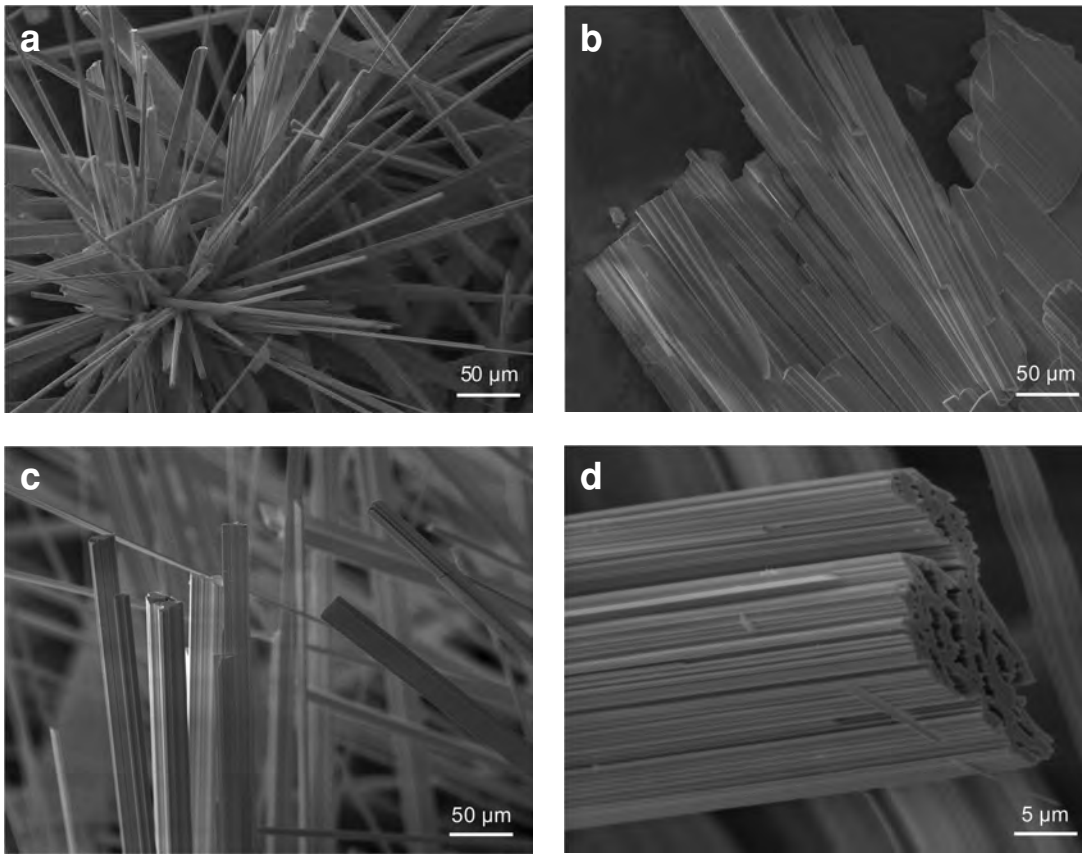

FIG. 3. SEM images of CVT grown sulfosalts: a) stoichiometric boulangerite (sample XE8D), b) Pb-poor boulangerite forming lamellae (sample B8–A), c) needles and hollow fibers of dadsonite, d) thin hollow wires of iodine-substituted pillaite.

days), *i.e.*, the CVT-grown boulangerite represents a non-equilibrium state.

Sections of dadsonite and iodine-substituted pillaite needles were also prepared for TEM parallel and perpendicular to their long axis in order to verify the XRD results and to check whether metal order exists or not. Dadsonite was clearly identified by TEM as a result of its typical rod-layer pattern if viewed along the fiber elongation (Fig. 4c). Two types of blocks, consisting of two parallel chain-like structure fragments of Me_5S_7 (for block 1) and Me_4S_6 (for block 2; both of "100-slab" type) adjoining each other include a chlorine atom supported by additional lead atoms for valence balance (see Fig. 5a). These "ropes" are interconnected by short fragments of the "311 slab" type (Makovicky *et al.* 2006). For dadsonite crystals oriented with the needle axis perpendicular to the direction of the electron beam, the diffraction patterns do not show additional reflections (Fig. 5e) that stem from metal order. Thus, the Sb,Pb mixed sites or the Sb split positions inside the inner rows of atoms in the Me_5S_7 chain fragments have no states of order in these synthetic crystals.

The structure of iodine-substituted pillaite (Fig. 5b, Kryukova *et al.* 2005) was derived from that of natural pillaite, which contains chlorine and oxygen (Meerschaut *et al.* 2001). The stoichiometry of the synthetic specimen, determined by TEM–EDX to be roughly $Pb_{9.6}Sb_{7.9}S_{23}I_{1.55}$, differs from the composition $Cu_{0.51}Pb_{8.73}Sb_{8.15}S_{20}I_{1.6}$ reported by Kryukova *et al.* (2005), because copper was excluded owing to CVT growth. However, both compositions exhibit a slightly higher Pb:Sb ratio than natural pillaite $Pb_9Sb_{10}S_{23}ClO_{0.5}$ (Orlandi *et al.* 2001) owing to a substitution of $Sb^{3+} + S^{2-}$ by $Pb^{2+} + I^-$, according to Doussier *et al.* (2008), for chloro-sulfosalts. Possible minor amounts of oxygen in the crystal structure of our synthetic material were not detectable by TEM–EDX. An HRTEM inspection of cross-sections of iodine-substituted pillaite fibers clearly identifies the characteristic chessboard-like arrangement (Fig. 5d), also in agreement with HRTEM image

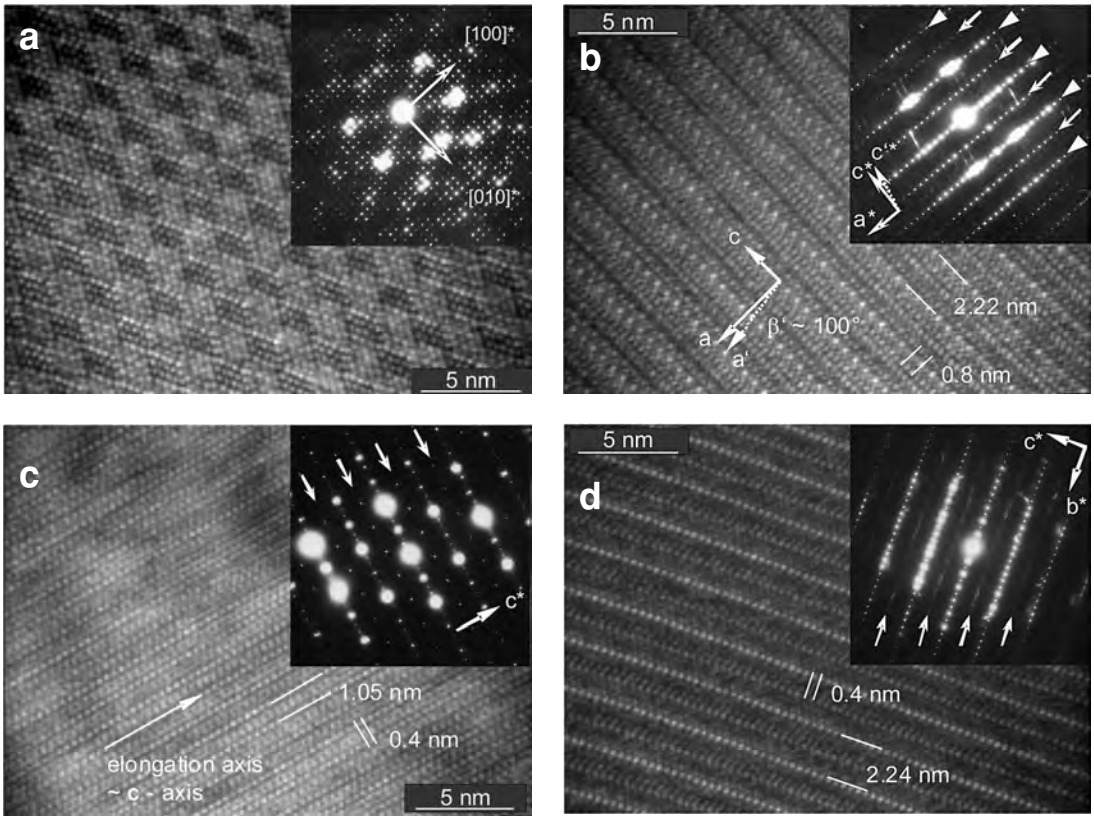

FIG. 4. HRTEM lattice images of: a, b) natural boulangerite $Pb_{5.1}Sb_{3.9}S_{10.95}$ from Trepça: a) beam direction (B) ∥ [001], *i.e.*, cross-section of a fiber; b) B ∥ [010]; owing to a well-established metal order between the reflection rows of the orthorhombic basic cell (marked by arrow tips), additional spots (marked by arrows) appear in the diffraction pattern (inset), which leads to the described monoclinic superstructure (labeled with *a*', *b*', *c*'*). Figures 4c and d show synthetic boulangerite. c) Sample B8–A $Pb_{4.82}Sb_{4.18}S_{11.09}$, Sb-rich boulangerite, B ∥ [320]; the additional weak reflection rows (inset) marked by arrows indicate metal order as well. d) Sample XE8D $Pb_5Sb_4S_{11}$ of ideal stoichiometry, B ∥ [100]; additional weak and diffuse reflection rows in SAED (inset) suggest an incomplete degree of metal order.

simulations based on the available structural data. The interatomic distances determined from cross-sections and sections parallel to the fiber axis (B ∥ [100], see Fig. 5f) agree well with the cell dimensions reported by Kryukova *et al.* (2005) and Meerschaut *et al.* (2001). Additional reflections (inset Fig. 6f) confirm the superstructure of 2•*b* (Kryukova *et al.* 2005). Probably, this is due to an ordered distribution of Pb and Sb on the mixed metal sites.

PHASE IDENTIFICATION AND DETERMINATION OF LATTICE PARAMETERS BY X-RAY DIFFRACTION

The crystalline phases of natural samples as well as CVT products were characterized by powder X-ray diffraction. Silicon (purity > 99.999%) was used as internal standard. Powdered CVT material was prepared on a zero-background sample holder (misoriented silicon wafer). For phase identification, the ICDD entries were used and ICSD entries for Rietveld refinements of unit-cell parameters and phase quantities. The Rietveld refinement includes the parameters of specimen displacement, polynomial background fitting ($0–5^{th}$ coefficient and 1/x term), scaling factors of each phase applied, preferred orientation of boulangerite by the March–Dollase function and, finally, the profile-function and the peak shape. The weighted profile-reliability factors R_{wp} and also R_{bragg} for the individual phases were found to be ≤10%, owing to strong textural effects in boulangerite.

Contrary to the sample from Příbram, the natural boulangerite from Trepça contains 11–15 wt.% galena (Fig. 6). Additional reflections at low diffraction-angles caused by ordered metal distribution were not observed.

The XRD powder patterns of the CVT products clearly show boulangerite. During the crystallization of Pb-poor materials, the phase $Pb_2Sb_2S_5$ formed in addition agrees well with the *d* values and cell parameters of the ICDD entry of "phase V" reported by Salanci (1979), as shown in Figure 6. Other available entries, as well as the crystal-structure data of Skowron & Brown (1990b), do not match the reflections observed. Thus we assume that "V" is a discrete phase. Dadsonite could be identified by means of its ICDD entries. For iodine-substituted pillaite, the identification was based on HRTEM and our own XRD measurements.

Comparing the corrected powder-diffraction pattern of different compositions of boulangerite, the peak positions are slightly shifted. As presented in Table 3, the refined unit-cell parameters of the boulangerite samples grown by CVT are related to the deviation of the atomic ratio Pb:Sb from the ideal value 1.25 for stoichiometric $Pb_5Sb_4S_{11}$. Because Pb is larger than Sb, the *c* parameter parallel to the needle axis decreases linearly with a lowering of Pb:Sb. The parameters *a* and *b* behave differently. Both increase for Pb:Sb larger than 1.25. But for Sb-rich compositions, *a* remains nearly unchanged, compared to that of a stoichiometric specimen, whereas *b* increases slightly. Obviously, the strong nonstoichiometry and consequent generation of metal vacancies lead to a distortion of the interatomic distances perpendicular to [001], the needle axis. However, the unit-cell volume shrinks continuously from Pb-rich toward Sb-rich synthetic boulangerite.

In spite of the similar absolute composition, the lattice parameters *b* and *c* of the natural boulangerite from Trepça and Příbram are larger than those of all synthetic ones. Although the *a* parameters are significantly smaller, the unit-cell volumes of the natural specimens are larger than those of the boulangerite samples grown by CVT. The strong degree of metal order in the natural specimens probably gives rise to this discrepancy. As mentioned above, the degree of metal order in synthetic crystals is rather weak or not detectable. However, the correlation of the *a* and *b* parameters with the ratio of Pb:Sb is valid as well, whereas *c* behaves in an opposite fashion.

TABLE 3. UNIT-CELL PARAMETERS OF BOULANGERITE AS A FUNCTION OF THE ATOM RATIO Pb/Sb

sample	Pb/Sb	*a* (Å)	*b* (Å)	*c* (Å)	*V* (Å³)
B8-G	1.30(4)	21.222(1)	23.470(1)	4.0308(3)	2007.7(3)
B8-D	1.27(4)	21.219(1)	23.467(1)	4.0301(3)	2006.8(3)
B8-F	1.19(4)	21.217(1)	23.468(1)	4.0292(2)	2006.2(3)
EL82	1.08(4)	21.217(1)	23.474(1)	4.0272(3)	2005.7(3)
Trepça	1.27(4)	21.185(1)	23.494(1)	4.0367(3)	2008.8(3)
Příbram	1.18(4)	21.181(1)	23.471(1)	4.0387(3)	2007.8(3)

The Electrical Conductivity of Boulangerite

As reported by Lomelino & Mozurkewich (1989), we found the electrical conductivity of natural and synthetic boulangerite $Pb_5Sb_4S_{11}$ to be roughly 10^{-6} $\Omega^{-1}m^{-1}$. They used water-dispersed graphite (Aquadag) to obtain contacts for measurements. For different sulfosalts and especially for crystals of small dimensions, we found that tinning solder consisting of Ga:In = 5:6 gives very reliable ohmic contacts, *e.g.*, for cylindrite (Kaden *et al.* 2010). It behaves as sputtered gold, but it is much better than conducting silver. Apparently, the liquid Ga–In alloy removes at T > 30°C impurities from the crystal surface because the surface is lightly dissolved. A heating at 80°C (one hour) was done to improve the contact behavior.

The electrical conductivity (at room temperature) of boulangerite strongly depends on the Pb:Sb ratio, as shown in Figure 7. From the lowest values of about $6(1) \times 10^{-8}$ $\Omega^{-1}m^{-1}$ for very Pb-poor samples El8–1, *i.e.*, $Pb_{4.65}Sb_{4.35}S_{11.18}$, the values rise with increasing Pb:Sb ratio up to about $5(1) \times 10^{-4}$ $\Omega^{-1}m^{-1}$ for the Pb-rich sample B8–G, $Pb_{5.1}Sb_{3.9}S_{10.95}$. Except for Pb-rich sample B8–G, all other samples show a more or less intense order of metals. Nevertheless, the values of this sample fit well with the average trend of σ depending on Pb:Sb. A functional dependence of the electrical conductivity on the specimen composition can be given by a linear regression as $\log \sigma = 13.5 \times$ (Pb:Sb) – 21.2 with a reliability factor of 0.95. Also, the value of σ for the boulangerite from Trepça, with its high degree of metal order, matches this function. Therefore, it seems that the order of metals does not influence significantly the electrical conductivity. The slightly higher conductivity of the Pb-poor boulangerite from Příbram may be attributed to impurities that were not clearly distinguishable by TEM–EDX. Outside the limit of stability of boulangerite, *e.g.*, for Pb:Sb = 1.02, the phase $Pb_2Sb_2S_5$ is stable and reaches again values as determined for Pb-rich boulangerite.

To prove the structurally defined anisotropy of charge-carrier transport, broader lamellae of the samples B8–A and EL8–3 were placed in contact in a manner that the conductivity can be measured parallel as well as perpendicular to their elongation. Since the lamellae are composed by many individual fibers intergrown parallel to [001], with each of them azimuthally misoriented against its neighboring fiber in a mosaic texture, the conductivity measured normal to the [001] should represent an average value over all directions belonging to the [001] zone. However, for both synthetic samples of boulangerite, the difference $\sigma_{\parallel} - \sigma_{\perp}$ was found to be negligible. More conspicuous is the dependence of σ of boulangerite on the Pb:Sb ratio (see above).

As experimentally found, the type of conduction in CVT-grown boulangerite could not be determined. However, if we assume, independently of the Pb:Sb

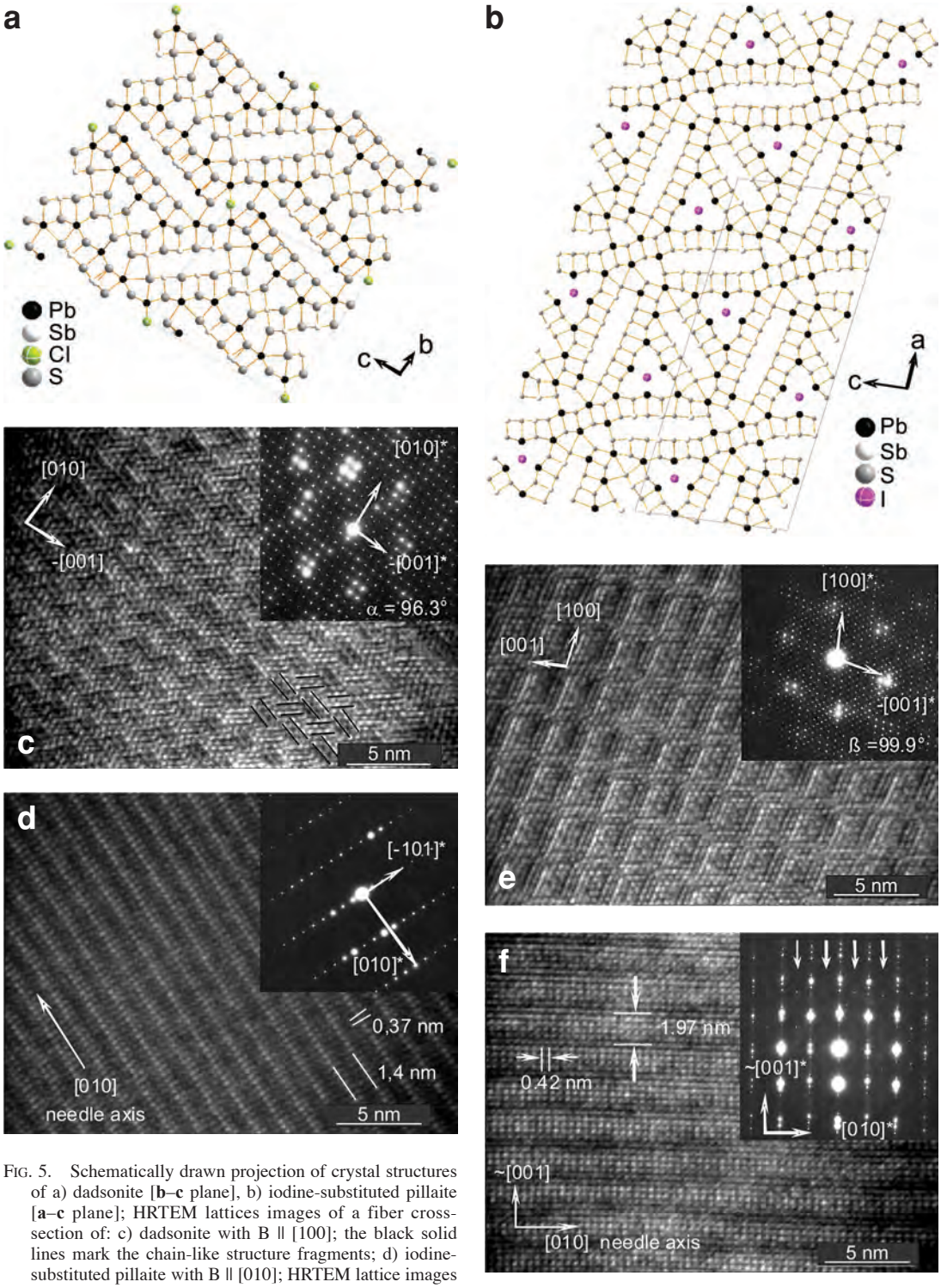

FIG. 5. Schematically drawn projection of crystal structures of a) dadsonite [**b**–**c** plane], b) iodine-substituted pillaite [**a**–**c** plane]; HRTEM lattices images of a fiber cross-section of: c) dadsonite with B ‖ [100]; the black solid lines mark the chain-like structure fragments; d) iodine-substituted pillaite with B ‖ [010]; HRTEM lattice images of a section parallel to the fiber axis of: e) dadsonite with B ‖ [101]; f) iodine-substituted pillaite with B ‖ [010].

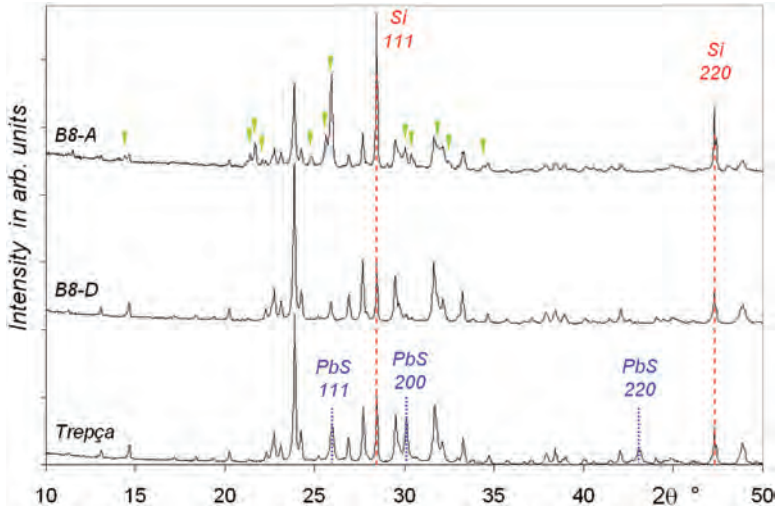

FIG. 6. XRD powder pattern of natural (Trepça) and synthetic (B8–D, B8–A) samples of boulangerite. The internal standard silicon is marked by dashed lines (online red); in the pattern of the natural sample, additional galena is indicated by dotted lines (online blue). Black triangles mark "phase V" $Pb_2Sb_2S_5$ in the pattern of B8–A.

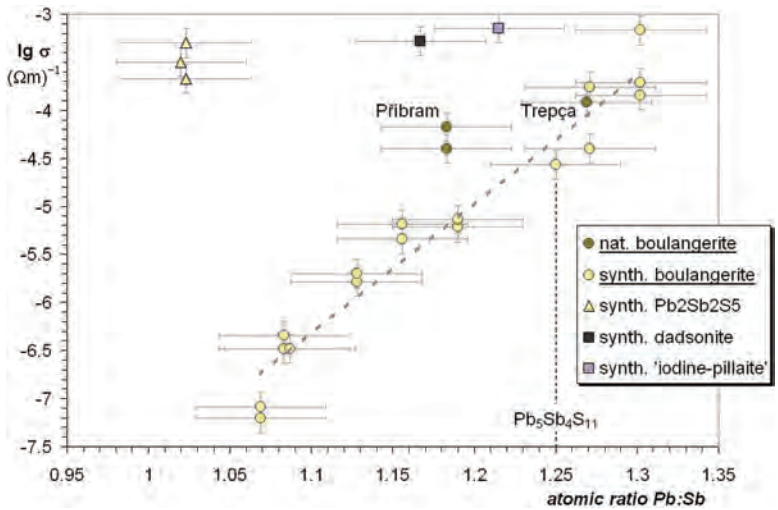

FIG. 7. Electrical conductivity σ at T = 298 K (in darkness) along the needle axis of various studied Pb–Sb sulfosalts. The dotted line is the linear regression of log σ for synthetic boulangerite: log σ = 13.5 × (Pb:Sb) – 21.2, with a reliability of 0.95. Note that the electrical conductivity of stibnite (Sb_2S_3) lies in the range of 10^{-7} – 10^{-5} $\Omega^{-1}m^{-1}$ (*e.g.*, Black *et al.* 1957, Lomelino & Mozurkewich 1989) and of galena (PbS) between 10^{-2} – 10^{2} $\Omega^{-1}m^{-1}$ (*e.g.*, Telkes 1950, Allgaier & Scanlon 1958).

ratio that boulangerite is an n-type conductor (negative Seebeck coefficients: Telkes 1950), the simple variation of the metal ratio Pb:Sb cannot serve as the only explanation for this dependence of σ on Pb:Sb. Crucial for this trend seems to be the heterovalent substitution of $Pb^{2+} \leftrightarrow Sb^{3+}$. As a consequence the

valence, balance with the sulfur sites is more or less lacking and, in addition, the lattice becomes distorted. If Sb (five valence electrons) replaces Pb (four valence electrons) in Pb-poor boulangerite, antimony acts as donor, according to eq. 4:

$$Pb^{2+} \leftrightarrow Sb^{3+}{}_{Pb} + e^{-}. \quad (4)$$

To satisfy the valence balance with the sulfur sites, metal vacancies (*e.g.*, V''_{Pb}) must be created, as is known for PbS (Masterov *et al.* 1999) and proposed for sulfosalts by Moëlo *et al.* (2008), where those metal vacancies act as acceptors:

$$3Pb^{2+} \leftrightarrow 2Sb^{3+}{}_{Pb} + V''_{Pb} \quad (5)$$

Both states should compensate each other. Thus, a decrease in the Pb:Sb ratio in boulangerite should lead to a decrease of the free carrier concentration due to self-compensation. A deterioration of conductivity should follow. For Pb:Sb > 1.25, *i.e.*, in Pb-rich boulangerite, lead replaces antimony and behaves as acceptor. On the one hand, the balance with the sulfur sites can be preserved by supplying sulfur vacancies, which act as donors:

$$2Sb^{3+} \leftrightarrow 2Pb^{2+}{}_{Sb} + V^{\bullet\bullet}_{S} \quad (6)$$

Such a formation of sulfur vacancies would indicate a decreased sulfur fugacity as well. Although in this case a self-compensation also is expected, the increased Pb:Sb ratio leads to increased values of σ, as shown in Figure 7. As the metal sites in the boulangerite structure act as donors, the sulfur sites behave as acceptors. If the boulangerite samples are really n-type conducting (independent of the Pb:Sb ratio), then the metals should dominate the conductivity. On the other hand, a decreased fugacity of sulfur could also lead to the formation of Sb–Sb bonds, *e.g.*, the pair $Sb^{4+}{}_2$, according to:

$$3Sb^{3+} \leftrightarrow Sb^{4+}{}_2 + Pb^{2+}{}_{Sb} \quad (7)$$

In this case, no sulfur vacancies are formed, and the lead on the antimony site acts as an acceptor. For the pair $Sb^{4+}{}_2$, there should not be a significant change of the electronic character compared to 2 Sb^{3+}. Thus, an increase of the charge-carrier transport and in σ is not plausible. Therefore, we assume a substitution according to equation 6; however, an additional examination of the antimony species will be necessary to provide an explicit evidence. Additional CVT experiments with a surplus of metallic Pb in the source material lead to the crystallization of metallic Sb in addition to boulangerite. Nevertheless, assuming that the phase $Pb_2Sb_2S_5$ is nearly stoichiometric, no lattice distortion and electronic self-compensation are expected. Hence, the electrical conductivity is comparable to that of stoichiometric boulangerite.

To prove an additional effect of illumination on the charge-carrier transport, some representative synthetic samples were measured in daylight. The resulting photoelectric response of these samples of boulangerite appears rather weak, with the ratio of illuminated to dark current I_{ill}/I_{dark} between 1.2 and 1.6, independently of the Pb:Sb ratio.

Conclusions

Boulangerite of different compositions within the homogeneity range $Pb_{5-x}Sb_{4+x}S_{11+x/2}$, as given by Salanci (1979), were produced by CVT over a temperature range between 400° and 600°C using NH_4Cl as the transporting agent. Optimum conditions for the crystallization of well-formed needles of boulangerite several mm in length were found to be at a deposition temperature of 570°C, ΔT ~ 37 K across a distance of 100 mm, and an initial NH_4Cl input of 0.033 mg/mL. A significant excess of Pb in the source material can lead to the crystallization of Pb-rich boulangerite in the deposition zone. If a stoichiometric reactant is used, boulangerite with a Pb:Sb ratio less than that of the starting material usually is formed, and $Pb_2Sb_2S_5$ ("phase V" of Salanci 1979) may appear as well. This is a result of the higher amount of mass transfer of gaseous antimony chlorides than of lead chlorides during CVT. This finding is supported by the thermochemical calculations of the equilibrium between the gaseous and condensed phases. In addition, the modeling of the thermochemical data predicts a slightly larger thermodynamic stability of Pb-poorer boulangerite. This finding correlates well with the observation that depending on the provenance, *e.g.*, Příbram, the natural samples of boulangerite are more or less Pb-poor. Moreover, the thermodynamic modeling of the transport reaction predicts a strong affinity of Pb for the halogens to form halogeno-sulfosalts at T < 470°C. Consequently, under these conditions, the CVT of boulangerite leads to the crystallization of chlorine-rich dadsonite, or to iodine-substituted pillaite if iodine is used as the transporting agent. A well-documented order among metals found in all natural samples of boulangerite studied leads to a monoclinic superstructure (Mumme 1989); it is only poorly developed for synthetic ones. Apparently, the comparatively short time of crystal growth during CVT prevents the complete ordering of metals, so that the synthetic boulangerite is in non-equilibrium. Whereas extremely Pb-poor specimens still show very weak order of metals, it is totally missing in Pb-rich boulangerite. The strongly ordered natural crystals have larger *b* and *c* parameters than the synthetic ones, whereas *a* is significantly smaller for similar compositions. For synthetic samples, the *c* dimension, *i.e.*, along the needle axis, decreases the more Pb is replaced by

Sb, together with a slight decrease of *a* and increase of *b*. The different behavior of *a* and *b* may be due to the generation of metal vacancies as a consequence of the heterovalent substitution of Pb^{2+} by Sb^{3+} to guarantee the balance of valences at the sulfur sites. These metal vacancies behave like acceptors and should compensate the donors formed by the Sb^{3+} on Pb^{2+} sites. Consequently, σ decreases by four orders of magnitude with a decrease of the Pb:Sb ratio, from 1.3 to about 1.07 (the lowest detected Pb:Sb ratio). The phase $Pb_2Sb_2S_5$ (Pb:Sb = 1) has an electrical conductivity σ similar to stoichiometric boulangerite, synthetic dadsonite and iodine-substituted pillaite.

Acknowledgements

This paper is dedicated to Emil Makovicky in recognition of his outstanding work in the field of sulfosalt research and structure systematics, especially, his particular descriptions of the unique architecture and modulated misfit layer-structure of cylindrite. His contributions inspired us to synthesize cylindrite microtubes and to study semiconducting properties of such compounds. We are indebted to the Department of Experimental Physics II for use their equipment for electrical characterization. H. Pöllmann (Institute of Geosciences, Mineralogy/Geochemistry group, Halle) is acknowledged for the generous permission to use the X'Pert powder diffractometer and the Rietveld software. Finally, we kindly thank the referees for the careful inspection of the manuscript and the very detailed and helpful annotations.

References

Allgaier, R.S. & Scanlon, W.W. (1958): Mobility of electrons and holes in PbS, PbSe and PbTe between room temperature and 4.2°K. *Phys. Rev.* **111**, 1029-1037.

Andersson, S. & Hyde, B.G. (1974): Twinning on the unit cell level as a structure-building operation in the solid state. *J. Solid State Chem.* **9**, 92-101.

Barin, I. (1992): *Thermochemical Data of Pure Substances*. 2. Auflage. Wiley-VCH Verlag, Weinheim, Germany.

Binnewies, M. & Milke, E. (1999): *Thermochemical Data of Elements and Compounds*. Wiley-VCH Verlag, Weinheim, Germany.

Black, J., Conwell E.M., Seigle, L. & Spencer C.W. (1957): Electrical and optical properties of some $M_2^{V-B}N_3^{VI-B}$ semiconductors. *J. Phys. Chem. Solids* **2**, 240-251.

Boldish, S.I. & White, W.B. (1998): Optical band gaps of selected ternary sulfide minerals. *Am. Mineral.* **83**, 865-871.

Born, L. & Hellner, E. (1960): A structural proposal for boulangerite. *Am. Mineral.* **45**, 1266-1271.

Carlson, E.H. (1972): Vapor phase crystal growth in the system PbS–Bi_2S_3. *J. Crystal Growth* **12**, 162-168.

Craig, J.R. & Barton, P.B., Jr. (1973): Thermochemical approximations for sulfosalts. *Econ. Geol.* **68**, 493-506.

Craig, J.R. & Lees, W.R. (1972): Thermochemical data for sulfosalt ore minerals; formation from simple sulfides. *Econ. Geol.* **67**, 373-377.

Cui Yi, Wie Qingqiao, Park Hongkun & Lieber, C.M. (2001): Nanowire nanosensors for highly sensitive and selective detection of biological and chemical species. *Science* **293**, 1289-1292.

Dirtu, D., Odochian, L., Pui, A. & Humelnicu, I. (2006): Thermal decomposition of ammonia. N_2H_4 – an intermediate reaction product. *Central Eur. J. Chem.* **4**, 666-673.

Dittrich, H., Bieniok, A., Brendel, U., Grodzicki, M. & Topa, D. (2007): Sulfosalts – a new class of compound semiconductors for photovoltaic applications. *Thin Solid Films* **515**, 5745-5750.

Dittrich, H. & Herz, K. (1998): Physical properties of ternary thin films based on sulfosalt compound. *Inst. Phys. Conf. Ser.* **152**, 293-296.

Dittrich, H., Stadler, A., Topa, D., Schimper, H.J. & Basch, A. (2009): Progress in sulfosalt research. *Phys. Stat. Sol.* **A206**, 1034-1041.

Doussier, C., Moëlo, Y., Meerschaut, A., Léone, P. & Guillot-Deudon, C. (2008): Crystal structure of the new compound $Pb_{3+x}Sb_{3-x}S_{7-x}Cl_{1+x}$ ($x \sim 0.45$): the homologous series $Pb_{(2+2N)}(Sb,Pb)_{(2+2N)}S_{(2+2N)}(S,Cl)_{(4+2N)}Cl_N$ and its polychalcogenide derivates (N = 1–3). *J. Solid State Chem.* **181**, 920-934.

Duan Xiangfeng, Huang Yu, Agarwal, R. & Lieber, C.M. (2003): Single-nanowire electrically driven lasers. *Nature* **421**, 241-245.

Eriksson, G. (1971): Thermodynamic studies of high temperature equilibria. *Acta Chem. Scand.* **25**, 2651-2658.

Fleischer, M. (1955): New mineral names. *Am. Mineral.* **40**, 1154-1155.

Ghosal, S. & Sack, R.O. (1999): Bi–Sb energetics in sulfosalts and sulfides. *Mineral. Mag.* **63**, 723-733.

Glaum, R., Gruehn, R. & Trappe, O. (1997): Programm CV Trans. University of Giessen, Germany.

Gruehn, R. & Schweizer, H.-J. (1983): Preparation of solid state compounds by chemical transport – interpretation and control using the cooperative transport model. *Angew. Chemie* **95**, 82-95.

Heuer, M., Wagner, G., Doering, T., Bente, K. & Kryukova, G. (2004): Nanowire arangements of PbS–Sb_2S_3-compounds. *J. Crystal Growth* **267**, 745-750.

HILLER, J.E. (1939): Über den Falkmanit. *Z. Kristallogr.* **102**, 138-142.

HYDE, B.G., BAGSHAW, A.N., ANDERSSON, S. & O'KEEFFE, M. (1974): Some defect structures in crystalline solids. *Annu. Rev. Mater. Sci.* **4**, 43-52.

JANAF Thermochemical Tables (1986) 3rd ed. American Chemical Society, American Institute of Physics, National Bureau of Standards, New York, N.Y.

KADEN, R., WAGNER, G., STRUM, C., SCHMIDT-GRUND, R., VON WENCKSTERN, H., PRAGER, A., BENTE, K. & GRUNDMANN, M. (2010): Synthesis and physical properties of cylindrite micro-tubes and lamellae. *Phys. Stat. Sol.* **247**, 1335-1350.

KITAKAZE, A., SUGAKI, A. & SHIMA, H. (1995): Study of the minerals on the PbS–Sb_2S_3 join. 1. Phase relations above 400°C. *Mineral. J.* **17**, 282-289.

KNACKE, O., KUBASCHEWSKI, O. & HESSELMANN, K. (1991): *Thermochemical Properties of Inorganic Substances*. Springer-Verlag, Berlin, Germany.

KRABBES, G., OPPERMANN, H. & WOLF, E. (1976): Der Transport von Bodenkörpern der Zusammensetzung $FeS_{1.00}$. *Z. anorg. allg. Chem.* **423**, 212-224.

KRYUKOVA, G., HEUER, M., WAGNER, G., DOERING, T. & BENTE, K. (2005): Synthetic $Cu_{0.507(5)}Pb_{8.73(9)}Sb_{8.15(8)}I_{1.6}S_{20.0(2)}$ nanowires. *J. Solid State Chem.* **178**, 376-381.

KUBASCHEWSKI, O. & ALCOCK, C.B. (1983): *Metallurgical Thermochemistry*. Pergamon Press, Oxford, U.K.

LEONTIDIS, E., ORPHANOU, M., KYPRIANIDOU-LEODIDOU, T. & KRUMEICH, F. (2003): Composite nanotubes formed by self-assembly of PbS nanoparticles. *Nano Letters* **3**, 569-572.

LOMELINO, T. F., MOZURKEWICH, G. (1989): Semiconducting band gaps of three lead–antimony sulfosalts. *Am. Mineral.* **74**, 1285-1286.

MAKOVICKY, E. (1977): Chemistry and crystallography of the lillianite homologous series. III. Crystal chemistry of lillianite homologues. Related phases. *Neues Jahrb. Mineral., Abh.* **131**, 187-207.

MAKOVICKY, E. (1985): The building principles and classification of sulphosalts based on the SnS archetype. *Fortschr. Mineral.* **63**, 45-89.

MAKOVICKY, E. (1989): Modular classification of sulphosalts – current status. Definition and application of homologous series. *Neues Jahrb. Mineral., Abh.* **160**, 269-297.

MAKOVICKY, E. (1993): Rod-based sulphosalt structures derived from the SnS and PbS archetypes. *Eur. J. Mineral.* **5**, 545-591.

MAKOVICKY, E. & KARUP-MØLLER, S. (1977a): Chemistry and crystallography of the lillianite homologous series. I. General properties and definitions. *Neues Jahrb. Mineral., Abh.* **130**, 264-287.

MAKOVICKY, E. & KARUP-MØLLER, S. (1977b): Chemistry and crystallography of the lillianite homologous series. II. Definition of new minerals: eskimoite, vikingite, ourayite and treasurite. Redefinition of schirmerite and new data on the lillianite–gustavite solid-solution series. *Neues Jahrb. Mineral., Abh.* **131**, 56-82.

MAKOVICKY, E. & TOPA, D. (2009): The crystal structure of sulfosalts with the boxwork architecture and their new representative, $Pb_{15-2x}Sb_{14+2x}S_{36}O_x$. *Can. Mineral.* **47**, 3-24.

MAKOVICKY, E., TOPA, D. & MUMME, W.G. (2006): The crystal structure of dadsonite. *Can. Mineral.* **44**, 1499-1512.

MASTEROV, V.F., NASREDINOV, F.S., SEREGIN, P.P., SEREGIN, N.P., ERMOLAEV, A.V. & BONDAREVSKIĬ, S.I. (1999): Determining the position of antimony impurity atoms in PbS by ^{119}Sb(^{119m}Sn) emission Mössbauer spectroscopy. *Semiconductors* **33**, 836-837.

MCQUEEN, K.G. (1987): A second occurrence of falkmanite: Pinnacles mine, Broken Hill, New South Wales. *Can. Mineral.* **25**, 15-19.

MEERSCHAUT, A. PALVADEAU, P. MOËLO, Y. & ORLANDI, P. (2001): Lead–antimony sulfosalts from Tuscany (Italy). IV. Crystal structure of pillaite, $Pb_9Sb_{19}S_{23}ClO_{0.5}$, an expanded monoclinic derivate of hexagonal $Bi(Bi_2S_3)_9I_3$, from the zinkenite group. *Eur. J. Mineral.* **13**, 779-790.

MOËLO, Y., MAKOVICKY, E., MOZGOVA, N.N., JAMBOR, J.L., COOK, N., PRING, A., PAAR, W., NICKEL, E.H., GRAESER, S., KARUP-MØLLER, S., BALIĆ-ŽUNIĆ, T., MUMME, G.W., VURRO, F., TOPA, D., BINDI, L., BENTE, K. & SHIMIZU, M. (2008): Sulfosalt systematics: a review. Report of the sulfosalt sub-committee of the IMA Commission on Ore Mineralogy. *Eur. J. Mineral.* **20**, 7-46.

MOH, G.H., BENTE, K. & MEIER-SALIMI, M. (1991): Thallium and gold: observations and experimental contributions to mineralogy, geochemistry and crystal chemistry. b) Substitution experiments and structure investigations on Ag–Tl-bearing boulangerites – a contribution to the rayite problem. *Neues Jahrb. Mineral., Abh.* **163**, 197-270.

MOZGOVA, N.N. & BORTNIKOV, N.S. (1980): Non-stoichiometry of acicular lead sulfosalts. *Int. Geol. Congress*, *26th* (*Moscow*), *Geokh. Mineral.*, 126-138 (in Russian).

MOZGOVA, N.N., BORTNIKOV, N.S., TSEPIN, A.I., BORODAEV, Y.S., VRUBLEVSKAJA, S.V., VYALSOW, L.N., KUZMINA, O.V. & SIVTSOV, A.V. (1983): Falkmanite, $Pb_{5.4}Sb_{3.6}S_{11}$, new data and relationship with sulphantimonites of lead (re-examination of type material from Bayerland mine, Bavaria). *Neues Jahrb. Mineral., Abh.* **147**, 80-98.

MOZGOVA, N.N., VRUVLEVSKAJA, S.V. & SIVTSOV, A.V. (1984): New data on the boulangerite homologous series. *Dokl. Akad. Nauk SSSR* **274**, 169-172 (in Russian).

MUMME, G.W. (1989): The crystal structure of $Pb_{5.05}(Sb_{3.75}Bi_{0.28})S_{10.72}Se_{0.28}$: boulangerite of near ideal composition. *Neues Jahrb. Mineral., Monatsh.*, 498-512.

ORLANDI, P., MOËLO, Y., MEERSCHAUT, A. & PALVADEAU, P. (2001): Lead–antimony sulfosalts from Tuscany (Italy). III. Pillaite, $Pb_9Sb_{19}S_{23}ClO_{0.5}$, a new Pb–Sb oxy-chloro-sulfosalt, from Buca della Vena mine. *Eur. J. Mineral.* **13**, 605-610.

PANalytical (2009): Program X'Pert HighScore Plus, version 3.0. PANalytical B.V., Almelo, The Netherlands.

PETROVA, I.V., KUZNETSOV, A.I., BELOKONEVA, E.L., SIMONOV, M.A., POBEDIMSKAYA, E.A. & BELOV, N.V. (1978): Crystal structure of boulangerite. *Dokl. Akad. Nauk SSSR* **242**, 337-340 (in Russian).

PRUSETH, K.L., MISHRA, B. & BERNHARDT, H.-J. (2001): The minerals boulangerite, falkmanite and Cu-free meneghinite: synthesis, new powder diffraction data and stability relations. *Eur. J. Mineral.* **13**, 411-419.

RAMDOHR, P. & ÖDMAN, O. (1940): Falkmanit, ein neues Bleispiessglanzerz, und sein Vorkommen, besonders in Boliden und Grube Bayerland. *Neues Jahrb. Mineral.* **A75**, 315-350.

ROBINSON, S.C. (1948): The identity of falkmanite and yenerite with boulangerite. *Am. Mineral.* **33**, 716-723.

SALANCI, B. (1979): Beiträge zum System PbS–Sb_2S_3 in Beziehung zu natürlichen Blei–Antimon-Sulfomineralien. *Neues Jahrb. Mineral., Abh.* **135**, 315-326.

SALANCI, B. & MOH, G.H. (1970): The pseudo-binary join galena–antimonite, PbS–Sb_2S_3. *Neues Jahrb. Mineral., Monatsh.*, 524-528.

SKOWRON, A. & BROWN, I. D. (1990a): Refinement of the structure of boulangerite, $Pb_5Sb_4S_{11}$. *Acta Crystallogr.* **C46**, 531-534.

SKOWRON, A. & BROWN, I. D. (1990b): Structure of $Pb_2Sb_2S_5$. *Acta Crystallogr.* **C46**, 534-536.

SKOWRON, A. & BROWN, I. D. (1994): Crystal chemistry and structures of lead–antimony sulfides. *Acta Crystallogr.* **B50**, 524-538.

STADELMANN, P. A. (1987): EMS – a software package for electron diffraction analysis and HREM image simulation in meterials science. *Ultramicroscopy* **21**, 131-145.

STADELMANN, P.A. (2008): Program JEMS, version 3.3425 U2008, CIME-EPFL, Lausanne, Switzerland.

STOE and Cie GmbH (2006): program STOE-X-AREA, version 1.35.

TELKES, M. (1950): Thermoelectric power and electrical resistivity of minerals. *Am. Mineral.* **35**, 536-555.

VRUBLEVSKAJA, S.V., MOZGOVA, N.N. & SIVTSOV, A.V. (1985): Structural characteristics of boulangerite homologues and their study with electron microdiffraction. *Izv. Acad. Nauk SSSR, Ser. Geol.* **4**, 90-97.

WANG, N. (1973): A study of the phases on the pseudobinary join PbS–Sb_2S_3. *Neues Jahrb. Mineral., Monatsh.*, 79-81.

WANG, N. (1976): Phases along the PbS–Sb_2S_3 join. *Neues Jahrb. Mineral., Abh.* **128**, 167-175.

YI, L.X., HEITMANN, J., SCHOLZ, R. & ZACHARIAS, M. (2002): Si rings, Si clusters, and Si nanocrystals – different states of ultrathin SiO_x layers. *Appl. Phys. Lett.* **81**, 4248-4251.

Received May 5, 2011, revised manuscript accepted May 7, 2012.

```
data_new21sua

_audit_creation_method            SHELXL-97
_chemical_name_systematic
;
 Lead Antimony sulfide (5.08/3.93/11)
;
_chemical_name_common             boulangerite
_chemical_melting_point           ?
_chemical_formula_moiety          'Pb5.08 Sb3.93 S11'
_chemical_formula_sum             'Pb5 S11 Sb4'
_chemical_formula_weight          1875.61

_chemical_special_details
;
The non-integer number of atoms in the unit-cell is due to the occurrence
of partially occupied sites and substitutional disorder.
;

loop_
 _atom_type_symbol
 _atom_type_description
 _atom_type_scat_dispersion_real
 _atom_type_scat_dispersion_imag
 _atom_type_scat_source
 'S'  'S'   0.1246   0.1234
 'International Tables Vol C Tables 4.2.6.8 and 6.1.1.4'
 'Sb'  'Sb'  -0.5866   1.5461
 'International Tables Vol C Tables 4.2.6.8 and 6.1.1.4'
 'Pb'  'Pb'  -3.3944  10.1111
 'International Tables Vol C Tables 4.2.6.8 and 6.1.1.4'

_symmetry_cell_setting            'monoclinic'
_symmetry_space_group_name_H-M    'P21/a'

loop_
 _symmetry_equiv_pos_as_xyz
 'x, y, z'
 '-x+1/2, y+1/2, -z'
 '-x, -y, -z'
 'x-1/2, -y-1/2, z'

_cell_length_a                    21.554(4)
_cell_length_b                    23.454(4)
_cell_length_c                    8.079(2)
_cell_angle_alpha                 90.00
_cell_angle_beta                  100.76(1)
_cell_angle_gamma                 90.00
_cell_volume                      4012.4(14)
_cell_formula_units_Z             8
_cell_measurement_temperature     293(2)
_cell_measurement_reflns_used     ?
_cell_measurement_theta_min       ?
_cell_measurement_theta_max       ?
```

```
_exptl_crystal_description        needle
_exptl_crystal_colour             silver
_exptl_crystal_size_max           1.2
_exptl_crystal_size_mid           0.10
_exptl_crystal_size_min           0.03
_exptl_crystal_density_meas       'not measured'
_exptl_crystal_density_diffrn     6.210
_exptl_crystal_density_method     'not measured'
_exptl_crystal_F_000              6320
_exptl_absorpt_coefficient_mu     48.217
_exptl_absorpt_correction_type    'empirical'
_exptl_absorpt_correction_T_min   0.2986
_exptl_absorpt_correction_T_max   0.7461
_exptl_absorpt_process_details    'program SADABS (Sheldrick 2008)'

_exptl_special_details
;
 ?
;

_diffrn_ambient_temperature       293(2)
_diffrn_radiation_wavelength      0.71073
_diffrn_radiation_type            MoK\a
_diffrn_radiation_source          'fine-focus sealed tube'
_diffrn_radiation_monochromator   graphite
_diffrn_measurement_device_type   'Bruker AXS X8 APEX2 CCD'
_diffrn_measurement_method        'integration of the spots (Apex suite)'
_diffrn_detector_area_resol_mean  ?
_diffrn_standards_number          ?
_diffrn_standards_interval_count  ?
_diffrn_standards_interval_time   ?
_diffrn_standards_decay_%         ?
_diffrn_reflns_number             118995
_diffrn_reflns_av_R_equivalents   0.1564
_diffrn_reflns_av_sigmaI/netI     0.0796
_diffrn_reflns_limit_h_min        -30
_diffrn_reflns_limit_h_max        30
_diffrn_reflns_limit_k_min        -33
_diffrn_reflns_limit_k_max        33
_diffrn_reflns_limit_l_min        -11
_diffrn_reflns_limit_l_max        10
_diffrn_reflns_theta_min          0.87
_diffrn_reflns_theta_max          30.58
_reflns_number_total              12443
_reflns_number_gt                 8495
_reflns_threshold_expression      >2sigma(I)

_computing_data_collection        'Apex program suite (Bruker 2003)'
_computing_cell_refinement        'Apex program suite (Bruker 2003'
_computing_data_reduction         'SAINT (Bruker 2003)'
_computing_structure_solution     'none'
_computing_structure_refinement   'SHELXL-97 (Sheldrick, 1997)'
_computing_molecular_graphics     ?
_computing_publication_material   ?
```

```
_refine_special_details
;
 Refinement of F^2^ against ALL reflections.  The weighted R-factor wR and
 goodness of fit S are based on F^2^, conventional R-factors R are based
 on F, with F set to zero for negative F^2^. The threshold expression of
 F^2^ > 2sigma(F^2^) is used only for calculating R-factors(gt) etc. and is
 not relevant to the choice of reflections for refinement.  R-factors based
 on F^2^ are statistically about twice as large as those based on F, and R-
 factors based on ALL data will be even larger.
;

_refine_ls_structure_factor_coef  Fsqd
_refine_ls_matrix_type            full
_refine_ls_weighting_scheme       calc
_refine_ls_weighting_details
 'calc w=1/[\s^2^(Fo^2^)+(0.0537P)^2^+334.9155P] where P=(Fo^2^+2Fc^2^)/3'
_atom_sites_solution_primary      direct
_atom_sites_solution_secondary    difmap
_atom_sites_solution_hydrogens    geom
_refine_ls_hydrogen_treatment     mixed
_refine_ls_extinction_method      none
_refine_ls_extinction_coef        ?
_refine_ls_number_reflns          12443
_refine_ls_number_parameters      360
_refine_ls_number_restraints      0
_refine_ls_R_factor_all           0.1161
_refine_ls_R_factor_gt            0.0623
_refine_ls_wR_factor_ref          0.1652
_refine_ls_wR_factor_gt           0.1351
_refine_ls_goodness_of_fit_ref    1.072
_refine_ls_restrained_S_all       1.072
_refine_ls_shift/su_max           0.000
_refine_ls_shift/su_mean          0.000

loop_
 _atom_site_label
 _atom_site_type_symbol
 _atom_site_fract_x
 _atom_site_fract_y
 _atom_site_fract_z
 _atom_site_U_iso_or_equiv
 _atom_site_adp_type
 _atom_site_occupancy
 _atom_site_symmetry_multiplicity
 _atom_site_calc_flag
 _atom_site_refinement_flags
 _atom_site_disorder_assembly
 _atom_site_disorder_group
A1 Pb 0.12228(5) 0.49872(4) 0.94540(18) 0.0228(2) Uani 1 1 d . . .
A2 Pb 0.30804(4) 0.15950(4) 0.02589(18) 0.01893(19) Uani 1 1 d . . .
A3 Pb 0.20558(4) 0.32436(3) 0.97843(18) 0.0205(2) Uani 1 1 d . . .
A4 Sb 0.46610(8) 0.43755(7) 0.3338(3) 0.0215(4) Uani 1 1 d . . .
A5A Pb 0.13286(13) 0.09657(11) 0.2035(5) 0.0225(5) Uiso 0.695(13) 1 d P . .
A5B Sb 0.1285(5) 0.1030(5) 0.200(2) 0.0225(5) Uiso 0.305(13) 1 d P . .
```

```
A6 Sb 0.37145(7) 0.30864(6) 0.3090(3) 0.0164(3) Uani 1 1 d . . .
A7 Sb 0.05948(8) 0.23021(7) 0.8996(4) 0.0263(4) Uani 1 1 d . . .
A8 Sb 0.48592(7) 0.12122(6) 0.3615(3) 0.0148(3) Uani 1 1 d . . .
A9 Sb 0.29219(7) 0.45695(6) 0.2789(3) 0.0220(4) Uani 1 1 d . . .
A1' Pb 0.11178(5) 0.49911(4) 0.42704(19) 0.0245(2) Uani 1 1 d . . .
A2' Pb 0.30543(4) 0.15990(4) 0.52952(18) 0.01987(19) Uani 1 1 d . . .
A3' Pb 0.20703(4) 0.32108(4) 0.4782(2) 0.0239(2) Uani 1 1 d . . .
A4' Pb 0.45191(5) 0.42983(4) 0.84862(19) 0.0248(2) Uani 1 1 d . . .
A5A' Pb 0.13455(16) 0.09449(16) 0.6919(6) 0.0239(6) Uiso 0.464(13) 1 d P . .
A5B' Sb 0.1262(3) 0.1049(3) 0.6779(9) 0.0239(6) Uiso 0.536(13) 1 d P . .
A6' Sb 0.38703(7) 0.28390(6) 0.8181(3) 0.0158(3) Uani 1 1 d . . .
A7' Pb 0.03872(5) 0.23296(4) 0.3978(2) 0.0268(2) Uani 1 1 d . . .
A8' Pb 0.48697(4) 0.13465(4) 0.86647(18) 0.01921(19) Uani 1 1 d . . .
A9' Sb 0.28390(7) 0.46674(6) 0.7692(3) 0.0174(3) Uani 1 1 d . . .
S1 S 0.0656(3) 0.0142(2) 0.8986(12) 0.0189(12) Uani 1 1 d . . .
S2 S 0.1866(3) 0.4165(2) 0.2198(11) 0.0159(11) Uani 1 1 d . . .
S3 S 0.2481(3) 0.0287(2) 0.0143(12) 0.0193(13) Uani 1 1 d . . .
S4 S 0.0968(3) 0.2940(3) 0.1548(13) 0.0241(15) Uani 1 1 d . . .
S5 S 0.1569(3) 0.1729(2) 0.9512(14) 0.0253(14) Uani 1 1 d . . .
S6 S 0.3338(3) 0.3747(2) 0.0649(10) 0.0195(14) Uani 1 1 d . . .
S7 S 0.4180(3) 0.2218(2) 0.0690(10) 0.0155(12) Uani 1 1 d . . .
S8 S 0.0149(3) 0.4450(2) 0.1533(11) 0.0192(14) Uani 1 1 d . . .
S9 S 0.3744(2) 0.0923(2) 0.3099(11) 0.0153(10) Uani 1 1 d . . .
S10 S 0.2766(3) 0.2494(2) 0.2666(11) 0.0144(11) Uani 1 1 d . . .
S11 S 0.0118(3) 0.1348(2) 0.1411(11) 0.0166(11) Uani 1 1 d . . .
S1' S 0.0712(3) 0.0182(2) 0.4172(11) 0.0163(11) Uani 1 1 d . . .
S2' S 0.1866(3) 0.4120(2) 0.7164(11) 0.0166(11) Uani 1 1 d . . .
S3' S 0.2448(3) 0.0285(2) 0.4793(11) 0.0184(13) Uani 1 1 d . . .
S4' S 0.0951(3) 0.2938(2) 0.6960(11) 0.0215(15) Uani 1 1 d . . .
S5' S 0.1549(3) 0.1759(2) 0.4548(14) 0.0235(14) Uani 1 1 d . . .
S6' S 0.3287(3) 0.3740(2) 0.5159(9) 0.0153(13) Uani 1 1 d . . .
S7' S 0.4198(3) 0.2192(3) 0.6047(10) 0.0172(13) Uani 1 1 d . . .
S8' S 0.0125(3) 0.4385(2) 0.6096(9) 0.0146(12) Uani 1 1 d . . .
S9' S 0.3676(3) 0.0847(2) 0.8122(11) 0.0161(11) Uani 1 1 d . . .
S10' S 0.2769(3) 0.2510(2) 0.7614(11) 0.0155(11) Uani 1 1 d . . .
S11' S 0.0172(3) 0.1389(2) 0.6306(12) 0.0197(12) Uani 1 1 d . . .

loop_
 _atom_site_aniso_label
 _atom_site_aniso_U_11
 _atom_site_aniso_U_22
 _atom_site_aniso_U_33
 _atom_site_aniso_U_23
 _atom_site_aniso_U_13
 _atom_site_aniso_U_12
A1 0.0302(5) 0.0160(4) 0.0233(6) -0.0030(5) 0.0081(5) -0.0029(3)
A2 0.0192(4) 0.0181(3) 0.0202(5) 0.0011(5) 0.0057(5) -0.0013(3)
A3 0.0206(4) 0.0185(4) 0.0231(6) 0.0006(5) 0.0062(5) 0.0018(3)
A4 0.0200(8) 0.0153(6) 0.0291(12) -0.0018(7) 0.0042(8) -0.0024(5)
A6 0.0172(6) 0.0124(6) 0.0195(9) 0.0016(7) 0.0032(8) 0.0001(5)
A7 0.0187(7) 0.0188(7) 0.0435(12) 0.0135(9) 0.0110(10) 0.0025(6)
A8 0.0200(7) 0.0084(5) 0.0173(9) -0.0009(7) 0.0071(8) -0.0010(5)
A9 0.0155(7) 0.0181(7) 0.0320(11) -0.0006(9) 0.0033(9) 0.0001(5)
A1' 0.0372(5) 0.0151(3) 0.0228(6) 0.0000(5) 0.0092(6) -0.0020(3)
A2' 0.0218(4) 0.0176(3) 0.0211(5) -0.0001(5) 0.0062(5) -0.0015(3)
```

```
A3' 0.0212(4) 0.0260(4) 0.0256(6) 0.0001(5) 0.0077(6) 0.0018(3)
A4' 0.0267(5) 0.0183(4) 0.0295(6) 0.0020(5) 0.0053(5) 0.0018(3)
A6' 0.0194(7) 0.0102(5) 0.0184(8) 0.0004(7) 0.0049(8) -0.0026(5)
A7' 0.0276(5) 0.0159(4) 0.0359(6) -0.0011(5) 0.0032(6) -0.0023(3)
A8' 0.0231(4) 0.0122(3) 0.0231(5) -0.0004(4) 0.0061(5) 0.0007(3)
A9' 0.0155(7) 0.0171(6) 0.0206(9) -0.0002(8) 0.0061(8) 0.0012(5)
S1 0.014(3) 0.020(2) 0.024(4) 0.001(3) 0.005(3) 0.0007(18)
S2 0.015(2) 0.013(2) 0.020(3) -0.002(3) 0.005(3) -0.0022(17)
S3 0.022(3) 0.013(2) 0.025(4) 0.005(3) 0.008(3) -0.001(2)
S4 0.017(3) 0.024(3) 0.033(5) -0.003(3) 0.007(3) -0.009(2)
S5 0.022(3) 0.010(2) 0.045(5) -0.001(3) 0.010(4) 0.0034(19)
S6 0.022(3) 0.015(2) 0.022(4) 0.005(3) 0.006(3) 0.000(2)
S7 0.018(3) 0.013(2) 0.016(3) 0.003(3) 0.004(3) -0.0028(18)
S8 0.018(3) 0.013(2) 0.029(4) -0.001(3) 0.010(3) -0.0044(19)
S9 0.012(2) 0.018(2) 0.015(3) 0.000(3) 0.002(3) 0.0025(18)
S10 0.019(3) 0.011(2) 0.016(3) -0.002(3) 0.009(3) -0.0012(17)
S11 0.021(3) 0.0107(19) 0.021(4) 0.003(3) 0.011(3) 0.0036(19)
S1' 0.017(2) 0.016(2) 0.016(3) 0.005(3) 0.003(3) 0.0042(18)
S2' 0.020(3) 0.015(2) 0.017(3) 0.001(3) 0.007(3) 0.0002(18)
S3' 0.016(3) 0.018(2) 0.021(4) -0.004(3) 0.003(3) 0.000(2)
S4' 0.026(3) 0.015(3) 0.024(5) 0.006(3) 0.006(3) -0.009(2)
S5' 0.012(2) 0.019(2) 0.041(4) -0.008(4) 0.009(4) 0.0046(19)
S6' 0.020(3) 0.013(2) 0.015(4) -0.003(2) 0.008(3) 0.0009(18)
S7' 0.017(3) 0.020(2) 0.017(4) -0.002(3) 0.007(3) -0.001(2)
S8' 0.019(3) 0.015(2) 0.011(3) 0.000(2) 0.004(3) -0.0018(19)
S9' 0.020(3) 0.009(2) 0.020(3) 0.001(3) 0.008(3) 0.0045(17)
S10' 0.020(3) 0.014(2) 0.015(3) 0.001(3) 0.008(3) 0.0017(18)
S11' 0.018(3) 0.018(2) 0.025(4) 0.004(3) 0.008(3) 0.004(2)

_geom_special_details
;
 All esds (except the esd in the dihedral angle between two l.s. planes)
 are estimated using the full covariance matrix.  The cell esds are taken
 into account individually in the estimation of esds in distances, angles
 and torsion angles; correlations between esds in cell parameters are only
 used when they are defined by crystal symmetry.  An approximate (isotropic)
 treatment of cell esds is used for estimating esds involving l.s. planes.
;

loop_
 _geom_bond_atom_site_label_1
 _geom_bond_atom_site_label_2
 _geom_bond_distance
 _geom_bond_site_symmetry_2
 _geom_bond_publ_flag
A1 S9' 2.790(7) 2_557 ?
A1 S3 2.840(6) 2_556 ?
A1 S9 3.022(7) 2_556 ?
A1 S2 3.067(7) 1_556 ?
A2 S7 2.751(6) . ?
A2 S9' 2.922(7) 1_554 ?
A2 S9 2.927(7) . ?
A2 S10' 3.014(7) 1_554 ?
A2 S10 3.029(7) . ?
A3 S2' 2.924(7) . ?
```

```
A3 S6 2.967(6) 1_556 ?
A3 S2 2.990(7) 1_556 ?
A3 S4 3.046(8) 1_556 ?
A3 S4' 3.060(8) . ?
A3 S10' 3.067(7) . ?
A3 S10 3.087(7) 1_556 ?
A4 S1' 2.468(6) 4_665 ?
A4 S1 2.598(8) 2_556 ?
A4 S11 2.616(7) 4_665 ?
A5A S11 2.716(6) . ?
A5A S5' 2.730(9) . ?
A5A S5 2.833(10) 1_554 ?
A5A S1' 2.998(8) . ?
A5B S11 2.580(13) . ?
A5B S5' 2.653(17) . ?
A5B S5 2.752(18) 1_554 ?
A6 S10 2.443(5) . ?
A6 S6 2.520(7) . ?
A6 S6' 2.562(7) . ?
A7 S4' 2.447(7) . ?
A7 S5 2.461(6) . ?
A7 S4 2.553(9) 1_556 ?
A8 S8' 2.425(7) 4_665 ?
A8 S8 2.453(7) 4_665 ?
A8 S9 2.457(5) . ?
A9 S2 2.430(6) . ?
A9 S6' 2.741(7) . ?
A9 S3' 2.802(8) 2_556 ?
A9 S6 2.846(7) . ?
A9 S3 2.904(8) 2 ?
A1' S9' 2.877(7) 2_556 ?
A1' S8' 3.019(6) 3_566 ?
A1' S8 3.023(7) . ?
A1' S9 3.025(7) 2_556 ?
A1' S3' 3.120(6) 2_556 ?
A2' S7' 2.796(6) . ?
A2' S10 2.968(7) . ?
A2' S9 2.976(7) . ?
A2' S10' 2.980(7) . ?
A2' S9' 2.997(7) . ?
A3' S6' 2.866(6) . ?
A3' S2' 2.960(7) . ?
A3' S10' 2.987(7) . ?
A3' S10 2.994(7) . ?
A3' S2 3.037(7) . ?
A4' S1 2.743(6) 4_665 ?
A4' S11 2.899(8) 4_666 ?
A4' S1 2.919(8) 2_557 ?
A4' S11' 2.935(8) 4_665 ?
A4' S1' 2.959(8) 2_556 ?
A5A' S11' 2.694(7) . ?
A5A' S5 2.762(10) . ?
A5A' S5' 2.797(10) . ?
A5A' S1' 2.978(8) . ?
A5A' S1 3.077(8) . ?
```

```
A5B' S11' 2.441(8) . ?
A5B' S5' 2.612(11) . ?
A5B' S5 2.705(11) . ?
A6' S10' 2.457(6) . ?
A6' S7 2.484(7) 1_556 ?
A6' S7' 2.495(7) . ?
A7' S5' 2.800(6) . ?
A7' S4' 2.867(8) . ?
A7' S4 2.896(9) . ?
A7' S11' 2.990(7) . ?
A7' S11 3.081(7) . ?
A8' S9' 2.787(6) . ?
A8' S8' 2.825(7) 4_665 ?
A8' S8 2.949(8) 4_666 ?
A8' S7' 3.060(7) . ?
A9' S2' 2.428(6) . ?
A9' S3' 2.459(8) 2_556 ?
A9' S3 2.470(8) 2_556 ?
S1 A4 2.598(8) 2_546 ?
S1 A4' 2.743(6) 4_565 ?
S1 A4' 2.919(8) 2_547 ?
S2 A3 2.990(7) 1_554 ?
S2 A1 3.067(7) 1_554 ?
S3 A9' 2.470(8) 2_546 ?
S3 A1 2.840(6) 2_546 ?
S3 A9 2.904(8) 2_545 ?
S4 A7 2.553(9) 1_554 ?
S4 A3 3.046(8) 1_554 ?
S5 A5B 2.752(18) 1_556 ?
S5 A5A 2.833(10) 1_556 ?
S6 A3 2.967(6) 1_554 ?
S7 A6' 2.484(7) 1_554 ?
S8 A8 2.453(7) 4_565 ?
S8 A8' 2.949(8) 4_564 ?
S9 A1 3.022(7) 2_546 ?
S9 A1' 3.025(7) 2_546 ?
S10 A3 3.087(7) 1_554 ?
S11 A4 2.616(7) 4_565 ?
S11 A4' 2.899(8) 4_564 ?
S1' A4 2.468(6) 4_565 ?
S1' A4' 2.959(8) 2_546 ?
S3' A9' 2.459(8) 2_546 ?
S3' A9 2.802(8) 2_546 ?
S3' A1' 3.120(6) 2_546 ?
S8' A8 2.425(7) 4_565 ?
S8' A8' 2.825(7) 4_565 ?
S8' A1' 3.019(6) 3_566 ?
S9' A1 2.790(7) 2_547 ?
S9' A1' 2.877(7) 2_546 ?
S9' A2 2.922(7) 1_556 ?
S10' A2 3.014(7) 1_556 ?
S11' A4' 2.935(8) 4_565 ?

loop_
 _geom_angle_atom_site_label_1
```

```
 _geom_angle_atom_site_label_2
 _geom_angle_atom_site_label_3
 _geom_angle
 _geom_angle_site_symmetry_1
 _geom_angle_site_symmetry_3
 _geom_angle_publ_flag
S9' A1 S3 78.12(19) 2_557 2_556 ?
S9' A1 S9 86.89(17) 2_557 2_556 ?
S3 A1 S9 75.52(19) 2_556 2_556 ?
S9' A1 S2 88.9(2) 2_557 1_556 ?
S3 A1 S2 76.75(19) 2_556 1_556 ?
S9 A1 S2 152.23(15) 2_556 1_556 ?
S7 A2 S9' 86.02(19) . 1_554 ?
S7 A2 S9 84.46(18) . . ?
S9' A2 S9 86.30(17) 1_554 . ?
S7 A2 S10' 77.55(18) . 1_554 ?
S9' A2 S10' 94.2(2) 1_554 1_554 ?
S9 A2 S10' 161.91(16) . 1_554 ?
S7 A2 S10 80.78(18) . . ?
S9' A2 S10 166.64(16) 1_554 . ?
S9 A2 S10 90.4(2) . . ?
S10' A2 S10 85.02(16) 1_554 . ?
S2' A3 S6 83.64(18) . 1_556 ?
S2' A3 S2 86.92(16) . 1_556 ?
S6 A3 S2 78.11(17) 1_556 1_556 ?
S2' A3 S4 119.16(19) . 1_556 ?
S6 A3 S4 138.4(2) 1_556 1_556 ?
S2 A3 S4 69.70(18) 1_556 1_556 ?
S2' A3 S4' 68.94(17) . . ?
S6 A3 S4' 146.1(2) 1_556 . ?
S2 A3 S4' 118.25(18) 1_556 . ?
S4 A3 S4' 74.59(18) 1_556 . ?
S2' A3 S10' 89.9(2) . . ?
S6 A3 S10' 79.26(18) 1_556 . ?
S2 A3 S10' 157.35(15) 1_556 . ?
S4 A3 S10' 130.36(16) 1_556 . ?
S4' A3 S10' 81.1(2) . . ?
S2' A3 S10 158.33(15) . 1_556 ?
S6 A3 S10 74.92(17) 1_556 1_556 ?
S2 A3 S10 91.67(19) 1_556 1_556 ?
S4 A3 S10 80.24(19) 1_556 1_556 ?
S4' A3 S10 129.52(15) . 1_556 ?
S10' A3 S10 83.13(15) . 1_556 ?
S1' A4 S1 90.6(2) 4_665 2_556 ?
S1' A4 S11 90.4(2) 4_665 4_665 ?
S1 A4 S11 95.5(3) 2_556 4_665 ?
S11 A5A S5' 86.6(2) . . ?
S11 A5A S5 87.5(2) . 1_554 ?
S5' A5A S5 94.3(2) . 1_554 ?
S11 A5A S1' 78.2(2) . . ?
S5' A5A S1' 91.4(3) . . ?
S5 A5A S1' 164.2(2) 1_554 . ?
S11 A5B S5' 91.0(5) . . ?
S11 A5B S5 92.0(5) . 1_554 ?
S5' A5B S5 97.9(4) . 1_554 ?
```

```
S10 A6 S6 95.8(2) . . ?
S10 A6 S6' 92.2(2) . . ?
S6 A6 S6' 92.34(19) . . ?
S4' A7 S5 94.7(3) . . ?
S4' A7 S4 95.4(2) . 1_556 ?
S5 A7 S4 93.0(3) . 1_556 ?
S8' A8 S8 98.6(2) 4_665 4_665 ?
S8' A8 S9 93.1(2) 4_665 . ?
S8 A8 S9 94.3(2) 4_665 . ?
S2 A9 S6' 89.8(2) . . ?
S2 A9 S3' 89.6(2) . 2_556 ?
S6' A9 S3' 91.2(2) . 2_556 ?
S2 A9 S6 90.4(2) . . ?
S6' A9 S6 82.00(16) . . ?
S3' A9 S6 173.2(2) 2_556 . ?
S2 A9 S3 86.5(2) . 2 ?
S6' A9 S3 170.0(2) . 2 ?
S3' A9 S3 98.09(17) 2_556 2 ?
S6 A9 S3 88.7(2) . 2 ?
S9' A1' S8' 80.89(17) 2_556 3_566 ?
S9' A1' S8 88.50(19) 2_556 . ?
S8' A1' S8 69.68(17) 3_566 . ?
S9' A1' S9 87.75(17) 2_556 2_556 ?
S8' A1' S9 71.80(16) 3_566 2_556 ?
S8 A1' S9 141.41(16) . 2_556 ?
S9' A1' S3' 74.83(18) 2_556 2_556 ?
S8' A1' S3' 137.55(15) 3_566 2_556 ?
S8 A1' S3' 142.0(2) . 2_556 ?
S9 A1' S3' 72.94(17) 2_556 2_556 ?
S7' A2' S10 82.06(18) . . ?
S7' A2' S9 82.91(18) . . ?
S10 A2' S9 90.62(19) . . ?
S7' A2' S10' 77.52(18) . . ?
S10 A2' S10' 84.45(16) . . ?
S9 A2' S10' 160.29(15) . . ?
S7' A2' S9' 82.93(18) . . ?
S10 A2' S9' 164.95(15) . . ?
S9 A2' S9' 86.48(16) . . ?
S10' A2' S9' 93.3(2) . . ?
S6' A3' S2' 82.17(17) . . ?
S6' A3' S10' 80.58(17) . . ?
S2' A3' S10' 90.8(2) . . ?
S6' A3' S10 75.97(16) . . ?
S2' A3' S10 158.05(15) . . ?
S10' A3' S10 83.88(16) . . ?
S6' A3' S2 76.51(17) . . ?
S2' A3' S2 84.03(16) . . ?
S10' A3' S2 156.98(15) . . ?
S10 A3' S2 92.6(2) . . ?
S1 A4' S11 83.1(2) 4_665 4_666 ?
S1 A4' S1 78.5(2) 4_665 2_557 ?
S11 A4' S1 83.1(2) 4_666 2_557 ?
S1 A4' S11' 80.5(2) 4_665 4_665 ?
S11 A4' S11' 90.66(18) 4_666 4_665 ?
S1 A4' S11' 158.74(17) 2_557 4_665 ?
```

```
S1 A4' S1' 78.2(2) 4_665 2_556 ?
S11 A4' S1' 161.16(16) 4_666 2_556 ?
S1 A4' S1' 90.38(17) 2_557 2_556 ?
S11' A4' S1' 89.1(2) 4_665 2_556 ?
S11' A5A' S5 84.6(2) . . ?
S11' A5A' S5' 82.6(2) . . ?
S5 A5A' S5' 92.1(2) . . ?
S11' A5A' S1' 79.1(2) . . ?
S5 A5A' S1' 163.0(2) . . ?
S5' A5A' S1' 90.5(3) . . ?
S11' A5A' S1 78.8(2) . . ?
S5 A5A' S1 91.7(3) . . ?
S5' A5A' S1 160.5(2) . . ?
S1' A5A' S1 80.56(18) . . ?
S11' A5B' S5' 91.6(3) . . ?
S11' A5B' S5 90.9(3) . . ?
S5' A5B' S5 97.7(3) . . ?
S10' A6' S7 94.1(2) . 1_556 ?
S10' A6' S7' 93.9(2) . . ?
S7 A6' S7' 98.0(2) 1_556 . ?
S5' A7' S4' 82.8(2) . . ?
S5' A7' S4 82.0(2) . . ?
S4' A7' S4 98.90(17) . . ?
S5' A7' S11' 77.5(2) . . ?
S4' A7' S11' 86.0(2) . . ?
S4 A7' S11' 158.14(18) . . ?
S5' A7' S11 78.7(2) . . ?
S4' A7' S11 159.15(18) . . ?
S4 A7' S11 87.9(2) . . ?
S11' A7' S11 80.82(17) . . ?
S9' A8' S8' 85.98(19) . 4_665 ?
S9' A8' S8 84.5(2) . 4_666 ?
S8' A8' S8 98.85(16) 4_665 4_666 ?
S9' A8' S7' 81.95(18) . . ?
S8' A8' S7' 91.03(19) 4_665 . ?
S8 A8' S7' 162.62(17) 4_666 . ?
S2' A9' S3' 95.2(2) . 2_556 ?
S2' A9' S3 95.1(2) . 2_556 ?
S3' A9' S3 99.8(2) 2_556 2_556 ?
A4 S1 A4' 96.7(2) 2_546 4_565 ?
A4 S1 A4' 89.16(17) 2_546 2_547 ?
A4' S1 A4' 101.5(2) 4_565 2_547 ?
A4 S1 A5A' 96.9(3) 2_546 . ?
A4' S1 A5A' 97.8(2) 4_565 . ?
A4' S1 A5A' 159.0(2) 2_547 . ?
A9 S2 A3 100.0(2) . 1_554 ?
A9 S2 A3' 98.2(2) . . ?
A3 S2 A3' 84.00(13) 1_554 . ?
A9 S2 A1 100.2(2) . 1_554 ?
A3 S2 A1 94.7(2) 1_554 1_554 ?
A3' S2 A1 161.5(2) . 1_554 ?
A9' S3 A1 99.9(2) 2_546 2_546 ?
A9' S3 A9 98.96(19) 2_546 2_545 ?
A1 S3 A9 95.1(2) 2_546 2_545 ?
A7 S4 A7' 98.45(19) 1_554 . ?
```

```
A7 S4 A3 85.0(3) 1_554 1_554 ?
A7' S4 A3 154.2(3) . 1_554 ?
A7 S5 A5B' 96.5(3) . . ?
A7 S5 A5B 98.6(4) . 1_556 ?
A5B' S5 A5B 101.0(3) . 1_556 ?
A7 S5 A5A' 102.3(3) . . ?
A5B' S5 A5A' 6.42(14) . . ?
A5B S5 A5A' 97.3(4) 1_556 . ?
A7 S5 A5A 101.7(3) . 1_556 ?
A5B' S5 A5A 99.5(2) . 1_556 ?
A5B S5 A5A 3.2(3) 1_556 1_556 ?
A5A' S5 A5A 95.47(19) . 1_556 ?
A6 S6 A9 91.9(3) . . ?
A6 S6 A3 95.1(2) . 1_554 ?
A9 S6 A3 91.6(2) . 1_554 ?
A6' S7 A2 96.5(2) 1_554 . ?
A8 S8 A8' 95.60(18) 4_565 4_564 ?
A8 S8 A1' 89.6(3) 4_565 . ?
A8' S8 A1' 148.5(2) 4_564 . ?
A8 S9 A2 107.7(2) . . ?
A8 S9 A2' 109.5(2) . . ?
A2 S9 A2' 87.44(14) . . ?
A8 S9 A1 99.7(2) . 2_546 ?
A2 S9 A1 85.8(2) . 2_546 ?
A2' S9 A1 150.7(2) . 2_546 ?
A8 S9 A1' 96.6(2) . 2_546 ?
A2 S9 A1' 155.5(2) . 2_546 ?
A2' S9 A1' 87.7(2) . 2_546 ?
A1 S9 A1' 86.73(14) 2_546 2_546 ?
A6 S10 A2' 104.1(2) . . ?
A6 S10 A3' 95.5(2) . . ?
A2' S10 A3' 92.8(2) . . ?
A6 S10 A2 101.8(2) . . ?
A2' S10 A2 85.74(13) . . ?
A3' S10 A2 162.5(2) . . ?
A6 S10 A3 93.8(2) . 1_554 ?
A2' S10 A3 161.9(2) . 1_554 ?
A3' S10 A3 83.09(13) . 1_554 ?
A2 S10 A3 92.9(2) . 1_554 ?
A5B S11 A4 99.5(4) . 4_565 ?
A5B S11 A5A 2.5(3) . . ?
A4 S11 A5A 97.5(2) 4_565 . ?
A5B S11 A4' 105.7(4) . 4_564 ?
A4 S11 A4' 89.23(18) 4_565 4_564 ?
A5A S11 A4' 104.2(2) . 4_564 ?
A5B S11 A7' 92.1(4) . . ?
A4 S11 A7' 97.4(3) 4_565 . ?
A5A S11 A7' 93.9(2) . . ?
A4' S11 A7' 159.8(2) 4_564 . ?
A4 S1' A4' 94.3(2) 4_565 2_546 ?
A4 S1' A5A' 102.7(2) 4_565 . ?
A4' S1' A5A' 162.5(2) 2_546 . ?
A4 S1' A5A 93.9(2) 4_565 . ?
A4' S1' A5A 92.5(3) 2_546 . ?
A5A' S1' A5A 82.50(16) . . ?
```

```
A9' S2' A3 104.2(3) . . ?
A9' S2' A3' 105.4(2) . . ?
A3 S2' A3' 86.94(14) . . ?
A9' S3' A9 98.9(2) 2_546 2_546 ?
A9' S3' A1' 98.9(2) 2_546 2_546 ?
A9 S3' A1' 95.5(2) 2_546 2_546 ?
A7 S4' A7' 97.2(2) . . ?
A7 S4' A3 86.5(2) . . ?
A7' S4' A3 153.1(3) . . ?
A5B' S5' A5B 94.6(3) . . ?
A5B' S5' A5A 92.7(2) . . ?
A5B S5' A5A 3.4(3) . . ?
A5B' S5' A5A' 5.33(14) . . ?
A5B S5' A5A' 93.0(4) . . ?
A5A S5' A5A' 90.93(19) . . ?
A5B' S5' A7' 95.7(3) . . ?
A5B S5' A7' 97.2(4) . . ?
A5A S5' A7' 100.2(3) . . ?
A5A' S5' A7' 100.9(3) . . ?
A6 S6' A9 93.4(2) . . ?
A6 S6' A3' 96.04(19) . . ?
A9 S6' A3' 95.5(2) . . ?
A6' S7' A2' 95.8(2) . . ?
A6' S7' A8' 94.3(3) . . ?
A2' S7' A8' 96.42(19) . . ?
A8 S8' A8' 102.01(19) 4_565 4_565 ?
A8 S8' A1' 97.5(2) 4_565 3_566 ?
A8' S8' A1' 94.30(18) 4_565 3_566 ?
A8' S9' A1 104.2(2) . 2_547 ?
A8' S9' A1' 98.4(2) . 2_546 ?
A1 S9' A1' 88.06(14) 2_547 2_546 ?
A8' S9' A2 98.6(2) . 1_556 ?
A1 S9' A2 90.3(2) 2_547 1_556 ?
A1' S9' A2 162.9(2) 2_546 1_556 ?
A8' S9' A2' 98.08(19) . . ?
A1 S9' A2' 157.7(2) 2_547 . ?
A1' S9' A2' 90.1(2) 2_546 . ?
A2 S9' A2' 85.02(13) 1_556 . ?
A6' S10' A2' 92.1(2) . . ?
A6' S10' A3' 107.5(2) . . ?
A2' S10' A3' 92.7(2) . . ?
A6' S10' A2 90.7(2) . 1_556 ?
A2' S10' A2 83.74(13) . 1_556 ?
A3' S10' A2 161.6(2) . 1_556 ?
A6' S10' A3 106.7(2) . . ?
A2' S10' A3 161.1(2) . . ?
A3' S10' A3 83.91(13) . . ?
A2 S10' A3 93.6(2) 1_556 . ?
A5B' S11' A5A' 4.08(16) . . ?
A5B' S11' A4' 106.3(3) . 4_565 ?
A5A' S11' A4' 102.5(2) . 4_565 ?
A5B' S11' A7' 94.7(3) . . ?
A5A' S11' A7' 98.7(2) . . ?
A4' S11' A7' 158.6(2) 4_565 . ?
```

```
_diffrn_measured_fraction_theta_max    0.997
_diffrn_reflns_theta_full              30.58
_diffrn_measured_fraction_theta_full   0.997
_refine_diff_density_max    5.098
_refine_diff_density_min   -6.044
_refine_diff_density_rms    1.016
```